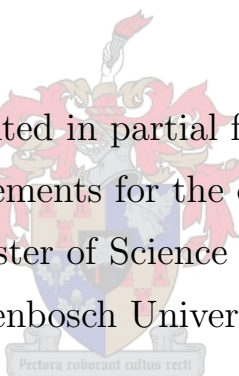


# Multi-detector Registration System for the Study of Multi-body Decay of Heavy Body Nuclei.

Vusi David Malaza

Thesis presented in partial fulfilment  
of the requirements for the degree of  
Master of Science  
at Stellenbosch University



Supervisor: Dr N. M. Jacobs  
Co-Supervisor: Prof Yu. V. Pyatkov  
Co-Supervisor: Dr D. V. Kamanin

December 2012

## Declaration

By submitting this thesis/dissertation electronically, I declare that the entirety of the work contained therein is my own, original work, that I am the sole author thereof (save to the extent explicitly otherwise stated), that reproduction and publication thereof by Stellenbosch University will not infringe any third party rights and that I have not previously in its entirety or in part submitted it for obtaining any qualification.

-----  
Vusi David Malaza

-----  
Date

## Abstract

Nuclear fission is commonly known as a process where a heavy nucleus such as Uranium or Thorium decays into two fragments of roughly equal mass. On occasion however, instead of decay into two parts a process known as binary fission, the nucleus can decay into three fragments. In this decay channel known as ternary fission, the nucleus splits into three fragments with the third particle being too light compared to the main fission fragments. There are also instances where heavy nuclei split into three fragments of comparable masses, the so called “true ternary fission” as was predicted by the theoretical calculations of *Strutinsky* [Str63]. While theoretical predictions hold promises for this decay mode, experimental attempts had little success in proving the existence of true ternary fission in low energy fission. The challenges and difficulties faced by experimentalist in confirming the existence of true ternary fission also proved that this fission mode is a very rare phenomenon.

This thesis is devoted to the investigation of ternary fission know as collinear cluster tripartition (CCT) in spontaneous fission of  $^{252}\text{Cf}$ , and the design and development of two time-of-flight spectrometers aimed at identifying all collinear multi-body decay partners directly. Prior to this study the only technique that was used at identifying decay partners in CCT was the “missing mass” approach. In this approach only two partners are identified directly with the third partner being identified by subtracting the two observed partners from the initial mass of the nucleus.

The experimental results from the two spectrometer setups showed that it was possible to identify all three partners of the CCT channel. The results also confirmed the existence of the so called “Sn lost” CCT mode which was already observed in earlier experiments.

## Acknowledgments

My greatest gratitude and hearty thanks goes to my supervisor and mentor Dr N.M. Jacobs for the guidance and supervision of my project. I am especially indebted to my supervisor for believing in me and for being there through each and every step of my academic career since I was an undergraduate. Most of all for his inspiration, great efforts and the good ideas throughout my project.

A special thanks goes to my supervisors from Russia, Prof Yu V. Pyatkov and Dr D.V. Kamanin for their time and knowledge they shared with me. Being around such brilliant world class physicists did not only help in developing me as a researcher and physicist but it also increased my passion and love for my discipline.

Experiments are not carried out by one person alone and to this end I would like to acknowledge my colleagues from the Flerov Laboratory for Nuclear Reactions (FLNR) of the Joint Institute for Nuclear Research (JINR) in Dubna, Russia: A.A. Aleksandrov, I.A. Aleksandrova, N.A. Kondratyev, E.A. Kuznetsova, O.V. Strelakovsky, A.O. Strelakovsky, V.E. Zhuchko and many others I might have missed to mention. A special thanks to V.E. Zhuchko for the programming experience I gained from you, N.A. Kondratyev for the hands-on experience when building the detectors, A.A. Aleksandrov and I.A. Aleksandrova for the exposure in all our experimental setups and vacuum systems and lastly but not least to Sasha (A.O. Strelakovsky) for being not only a colleague to me but also a friend, thank you very much.

I would also like to acknowledge the SA-JINR Collaboration, the Department of Science and Technology (DST), the National Research Foundation (NRF) and the Joint Institute

for Nuclear Research (JINR) through the office of the Deputy Head of the JINR office of Science Coordination and International Cooperation Dr D.V. Kamanin for the financial support and for the opportunity of being the first student to deliver a Masters thesis through the SA-JINR collaboration.

I wish to thank the Dean of Faculty of Military Science of Stellenbosch University, Prof M.S. Tshehla for his motivation and support of my work.

Let me also take this opportunity to thank the members of the Physics Department at Military Academy for taking up my classes and other departmental duties during my absence to Russia and to all the members of the School of Science and Technology.

I would also like to thank my friends at Military Academy, Lorraine “Lolo” Dichabe my office neighbour for the well-deserved tea times, Lindiwe “Lindi” Mashigo my psychologist for the lunch times you never missed, Nontlahla “Minky” Dywili for the moral and emotional support, and Alfred “Ali” Sehone for being a very good friend, partner, colleague, brother, etc. To all of you guys, thank you.

To my best friend *Thabile “Small” Mbuli*, you still the best, I thank you for everything.

More on the personal note I wish to thank my family. To my parents, thanks for the prayers and support, especially *uMamaThandi* for the life time dream she has for me, to my brother *Tawa* thanks for the all time advices, to my sister *Malindi* thanks for the family support and love, and to my younger sister *Thandi* thanks for the swag you have for me.

Lastly I would like to thank “*uNdlunkulu*”: Reabetswe Charmaine Selomo, for being a mother to Kagiso and look after him every time I was gone to Russia. Thank you for the perseverance and personal support and mostly for being there for me, it made you deserve to be “*uNdlunkulu wakwami*”.

To God The Almighty, your word in the book of Psalm 118:1 says “*Give thanks to the lord, for He is good; His love endures forever*”, I just want to do just that. Thank you God for everything.

This thesis is dedicated to my firstborn baby girl  
*Olebogeng Lesego Malaza.*

## List of Publications

The results of the present work have been reported at different conferences and have also been published in several scientific papers. Below is the list of publications and conference presentations that constitutes the results of this work:

1. *D.V.Kamanin, Yu.V.Pyatkov, E.A.Kuznetsova, A.A.Alexandrov, I.A.Alexandrova, S.B.Borzakov, M.L.Chelnokov, D.Fam Min, N. Jacobs, V. Malaza, N.A.Kondratyev, Yu.N.Kopatch, Ts.Panteleev, Yu.E.Penionzhkevich, Yu.V. Ryabov, A.I.Svirikhin, E.A.Sokol, D.A.Testov, V.E.Zhuchko, A.V.Yeremin*

**Collinear cluster tripartition as a neutron source - evaluation of the setup parameters**

International Symposium on Exotic Nuclei, Sochi, Russia, 28 September - 2 October 2009. Conference proceedings. Editors: Yu.E.Penionzhkevich, and S.M.Lukyanov. AIP Conference Proceedings, 2010, p. 385-392.

2. *D.V.Kamanin, Yu.V.Pyatkov, W. von Oertzen, A.A.Alexandrov, I.A.Alexandrova, O.V.Falomkina, N.Jacobs, N.A.Kondratjev, Yu.N.Kopatch, E.A.Kuznetsova, Yu.E.Lavrova, V.Malaza, S.Mullins, A.N.Tyukavkin, W.Trzaska and V.E.Zhuchko*

**Multi-cluster decays of heavy nuclei - studies in progress**

Proceedings of the 2nd SOUTH AFRICA - JINR Symposium "Models and Methods in Few- and Many-Body Systems", Dubna, Russia, 8-10 September 2010. Dubna 2010, p. 179-193.

3. *V. Malaza, N Jacobs, D.V.Kamanin, Yu.V.Pyatkov*

**Estimation of parameters of the "neutron belt" of the COMETA Setup**

**using the experimental data**

Presented in the 55th Annual Conference of the SA Institute of Physics in Pretoria (2010)

4. *Yu.V.Pyatkov, D.V.Kamanin, A.A.Aleksandrov, I.A.Aleksandrova, N.A.Kondratyev, E.A.Kuznetsova, N.Jacobs, V.Malaza, D.Pham Minh, V.E.Zhuchko*

**Presumable scenario of one of the collinear cluster tri-partition modes**

Proceedings of the International Workshop on State of the Art in Nuclear Cluster Physics “SOTANCP 2010” Brussels, Belgium, 25-28 May 2010. Int. Journal of Modern Physics E. 2011. V. 20, No. 4. p. 1008-1011.

5. *D.V.Kamanin, Yu.V.Pyatkov, A.A.Alexandrov, I.A.Alexandrova, S.B.Borzakov, N.Jacobs, N.A.Kondratyev, Yu.N.Kopach, E.A.Kuznetsova, V.Malaza, Ts.Panteleev, D.Pham Minh, V.E.Zhuchko*

**Collinear cluster tri-partition of  $^{252}\text{Cf}(sf)$  - evidences in neutron gated data**

Proceedings of the 18th International Seminar on Interaction of Neutrons with Nuclei: “Neutron Spectroscopy, Nuclear Structure, Related Topics”. Dubna, 26-29 May 2010. Dubna 2011, p. 102-107.

6. *D.V.Kamanin, Yu.V.Pyatkov, V.Malaza, A.A.Alexandrov, I.A.Alexandrova, N.Jacobs, N.A.Kondratyev, E.A.Kuznetsova, O.V.Strekalovsky, A.O.Strekalovsky, V.E.Zhuchko*

**Studying of some rare modes of collinear cluster tri-partition of  $^{252}\text{Cf}(sf)$** 

Presented at the 19th International Seminar on Interaction of Neutrons with Nuclei, Dubna, Russia, 25-28 May 2011.

7. *D.V.Kamanin, Yu.V.Pyatkov, A.A.Alexandrov, I.A.Alexandrova1, N.Jacobs, N.A.Kondratyev, E.A.Kuznetsova, V.Malaza, O.V.Strekalovsky, V.E.Zhuchko*

**Collinear cluster tri-partition: current status of studies**

Proceedings of the 19th International Seminar on Interaction of Neutrons with Nuclei, Dubna, Russia, 25-28 May 2011. Dubna 2012, p. 48-55.

8. *V. Malaza, N Jacobs, D.V.Kamanin, Yu.V.Pyatkov*

**Study of rare modes of Collinear Cluster Tripartition of  $^{252}\text{Cf}(sf)$**



Proceedings of the 56th Annual Conference of the SA Institute of Physics in Pretoria, South Africa (2011)

9. *D.V. Kamanin, Yu.V. Pyatkov, N.A. Kondratyev, V.E. Zhuchko, A.A. Alexandrov, I.A. Alexandrova, N. Jacobs, E.A. Kuznetsova, V. Malaza, S.I. Mulgin, O.V. Strelalovsky*  
**Mosaics Time-of-Flight COMETA Spectrometer for the study of multi-body decays of heavy niclei.**  
 Presented at the 7th International Conference on Dynamical Aspects of Nuclear Fission “DANF2011”, Smolenice Castle, Slovak Republic, 17-21 October 2011.
10. *D.V.Kamanin, Yu.V.Pyatkov, V.Malaza, A.A.Alexandrov, I.A.Alexandrova, N.Jacobs, N.A.Kondratyev, E.A.Kuznetsova, O.V.Strelalovsky, A.O.Strelalovsky, V.E.Zhuchko*  
**Study of rare modes of “Collinear Cluster Tri-partition” of  $^{252}\text{Cf}(sf)$**   
 Proceedings of the 19th International Seminar on Interaction of Neutrons with Nuclei, Dubna, Russia, 25-28 May 2011. Dubna, 2012, p. 56-61.
11. *D.V.Kamanin, Yu.V.Pyatkov, N.A.Kondratyev, V.E.Zhuchko, A.A.Alexandrov, I.A.Alexandrova, N.Jacobs, E.A.Kuznetsova, V.Malaza, S.I.Mulgin, A.O.Strelalovsky, O.V.Strelalovsky*  
**COMETA spectrometer for studying of multi-body decays of heavy nuclei**  
 Presented at the 20th International Seminar on Interaction of Neutrons with Nuclei, Alushta, Ukraine, 21-26 May 2012.
12. *D.V.Kamanin, Yu.V.Pyatkov, A.A.Alexandrov, I.A.Alexandrova, N.Jacobs, N.A.Kondratyev, E.A.Kuznetsova, V.Malaza, Yu.V.Ryabov, O.V.Strelalovsky, V.E.Zhuchko*  
**Summary of experimental results on collinear cluster tri-partition studies**  
 Presented at the 20th International Seminar on Interaction of Neutrons with Nuclei, Alushta, Ukraine, 21-26 May 2012.
13. *Yu.V.Pyatkov, D.V.Kamanin, W. von Oertzen, A.A.Alexandrov, I.A.Alexandrova, O.V.Falomkina, N.Jacobs, N.A.Kondratjev, E.A.Kuznetsova, Yu.E.Lavrova, V.Malaza, Yu.V.Ryabov, O.V.Strelalovsky, A.N.Tyukavkin and V.E.Zhuchko*  
**The collinear cluster tri-partition (CCT) of  $^{252}\text{Cf}(sf)$ : New aspects from neutron gated data** Eur. Phys. J. A: Hadrons and Nuclei. 2012. V. 48, No. 7. pp. 94109.

# Contents

<b>1</b>	<b>Introduction</b>	<b>1</b>
1.1	Nuclear Fission . . . . .	1
1.2	Ternary Fission . . . . .	2
1.2.1	Conventional Ternary Fission . . . . .	2
1.2.2	Polar Emission . . . . .	3
1.2.3	True Ternary Fission . . . . .	5
1.3	Collinear Cluster Tri-partition . . . . .	6
1.3.1	Experimental Evidence of the Collinear Cluster Tri-partition . . . . .	8
1.3.2	“Sn-lost” CCT mode . . . . .	16
1.4	Conclusion . . . . .	22
<b>2</b>	<b>Experimental Setups and Techniques</b>	<b>24</b>
2.1	Introduction . . . . .	24
2.2	Overview of the Si Detector Based Mosaic Spectrometers . . . . .	25
2.3	Motivation for using Mosaic Spectrometers in the study of the CCT phenomena. . . . .	25
2.4	COMETA Setup . . . . .	27

---

2.4.1	Description of the COMETA setup . . . . .	27
2.4.2	“Neutron belt” of the COMETA . . . . .	27
2.4.3	Electronics . . . . .	30
2.5	Light Ions Spectrometer . . . . .	32
2.5.1	Physical Motivation . . . . .	32
2.5.2	Description of the LIS Setup . . . . .	34
2.5.3	Electronics of the LIS Setup . . . . .	35
2.6	Data Acquisition System . . . . .	37
2.6.1	WinELTEC . . . . .	39
2.6.2	Mini-Client . . . . .	39
2.6.3	Htask . . . . .	39
2.6.4	Hoopsy32 . . . . .	39
2.6.5	HopRead32 . . . . .	40
<b>3</b>	<b>Data Analysis</b>	<b>41</b>
3.1	Introduction . . . . .	41
3.2	Detection Efficiency of the “Neutron Belt” of the COMETA Setup . . . . .	42
3.2.1	Modeling of the “Neutron Belt” . . . . .	42
3.2.2	Calculating the Detection Efficiency of the “Neutron Belt” Using Experimental Data . . . . .	43
3.3	Data Stability . . . . .	49
3.3.1	Results of Data Stability Test . . . . .	50

---

3.4	Reconstruction of the Fission Fragment Masses . . . . .	51
3.4.1	The “First Approximation” Approach . . . . .	52
3.4.2	True Energy Calibration and Reconstruction of FF Masses . . . . .	54
3.5	“Plasma Delay” and Correctness of the Velocity Measurement . . . . .	58
3.5.1	“Plasma Delay” . . . . .	58
3.5.2	“Plasma Delay” Correction . . . . .	60
<b>4</b>	<b>Results and Conclusion</b>	<b>61</b>
4.1	Introduction . . . . .	61
4.2	The First Experimental Results from LIS setup . . . . .	61
4.3	Conclusion . . . . .	68
4.3.1	Summary . . . . .	68
4.3.2	Conclusion . . . . .	69
4.3.3	Future work . . . . .	69

# List of Figures

1.1	Mass distribution of $^{252}\text{Cf}$ fission fragments obtained from [Now82]. . . . .	5
1.2	The potential energy of absolute equilibrium shapes for the conventional sequence of shapes (1 and 2), two-neck shapes (3) and three-neck shapes (4) [Str63]. . . . .	7
1.3	Schematic view of the modified FOBOS setup. . . . .	9
1.4	The overall view of FOBOS spectrometer with a belt of neutron counters. . . . .	9
1.5	A scheme of the experiment performed at the FOBOS setup for coincidence measurement of two fragments of the CCT partners for $^{252}\text{Cf}$ [Pya10]. . . . .	10
1.6	Contour map of the mass-mass distribution of the collinear fragments detected in coincidence in the two opposite arms of the FOBOS spectrometer setup [Pya10]. . . . .	11
1.7	Distribution which shows a contour map of the difference between the tails 3 and 4 in Fig 1.6 . . . . .	13
1.8	Shows the same distribution as in Fig 1.7 but a second derivative filter has been applied to emphasize the local peaks in each section of the $M_s = \text{constant}$ . . . . .	15
1.9	Parameters of Lead Radioactivity in comparison with those of CCT [Pya10]. . . . .	16
1.10	A scheme (a) and a photo (b) of the setup performed at JYFL. . . . .	17

1.11	Mass-mass distribution of fragments selected by velocities and energies for the “Sn-lost” CCT mode. . . . .	18
1.12	Mass spectrum for the structures marked by red lines in Fig 1.11 . . . . .	19
1.13	Schematic pre-scission configuration of the CCT mode based on the double magic $^{132}\text{Sn}$ cluster. . . . .	20
1.14	Potential energy of the fissioning nucleus of $^{252}\text{Cf}$ corresponding to the bottom of the potential valleys as a function of a parameter Q proportional to the quadrupole moment [Pya10a]. . . . .	21
2.1	Scheme of the COMETA which consist of two mosaics of PIN-diodes (4), MCP based “start” detector (2) with $^{252}\text{Cf}$ inside (1) and a “neutron belt”(3) that consist of 28 $^3\text{He}$ -filled neutron counters. The configuration of the belt is shown on the insert marked by the arrow. . . . .	28
2.2	a) Overall view of the COMETA and the “neutron belt” b) MCP “start” detector and mosaics of PIN diodes mosaic. . . . .	29
2.3	Detector modules for Neutron counters. a) Shows the moderator, b) Neutron counter with high voltage input and preamplifier, c) the Neutron counter inside the modulator. . . . .	31
2.4	Scheme for the electronics of the COMETA Spectrometer. . . . .	33
2.5	Schematic view of LIS setup. . . . .	34
2.6	Side and front view of the detector system of the LIS setup. . . . .	35
2.7	Overview of the LIS setup, the connections of the detector system inside the vacuum chamber shown in (a), the data acquisition system shown in (b), and the overview of the LIS setup and some of the electronics shown in (c). . . . .	36
2.8	Scheme for the electronics for LIS setup. . . . .	38

3.1	Comparing the experimental data with the calculated distribution at $\varepsilon = 4.25\%$ . . . . .	45
3.2	Algorithm for the entire process to obtain the calculated distributions. . .	46
3.3	Number of detected neutrons from fission events only with no background.	47
3.4	Comparison between the distribution with background neutrons and without background neutrons. . . . .	48
3.5	Mean value $\mu_T$ of time channel from PIN-21 versus the group of events. . .	50
3.6	Illustration of first approximation energy calibration. . . . .	53
3.7	The “first approximation” approach in the FF masses reconstruction. . . .	55
3.8	The “true energy calibration” approach and reconstruction of FF masses. .	59
3.9	Illustration of “plasma delay” for heavy ions ( $HI$ ) compared to protons ( $p$ ) as defined in [Han78] and [Nei83]. . . . .	60
4.1	The mass spectra obtained from LIS setup through the true calibration procedure compare to the known mass spectrum from literature [Wah88]. .	62
4.2	Velocity spectra from the two arms compared with literature spectrum [Sch83].	64
4.3	The velocity from the MCP-MCP time of flight versus the velocity from the PIN-MCP time of flight of the first arm. . . . .	65
4.4	The velocity from the MCP-MCP time of flight versus the velocity from the PIN-MCP time of flight of arm two. . . . .	66
4.5	A mass versus mass distribution of the events selected by the W1 and W2 gates. . . . .	67

# List of Tables

3.1	Different configurations to arrange neutron counters in the belt. .	43
3.2	Probability of emission of $n$ neutrons in $^{252}\text{Cf}$ source. . . . .	44
4.1	Parameters obtained from the first experiment using LIS setup. .	63
4.2	Comparison of the velocity and energy parameters of the LIS setup with results from literature. . . . .	63



# Chapter 1

## Introduction

### 1.1 Nuclear Fission

Soon after *Fermi* and his collaborators discovered that neutrons can be the most effective projectile in nuclear reactions and mostly in producing new heavier elements [Fer34], there was an increase in the interest for finding nuclei of higher mass, and charge number more than the one which was already known at that time. *Fermi* discovered that if the heaviest known element, in his case, uranium is bombarded with neutrons, it is possible to produce new elements with atomic number greater than that of uranium. In 1939, *Hahn* and *Strassmann* following up on *Fermi's* work discovered that uranium bombarded with neutrons sometimes produces smaller nuclei that are approximately half the size of the original uranium nucleus [Hah39]

Experimental work carried out by *Meitner* and *Frisch* on the *Disintegration of Uranium by Neutrons* revealed that the uranium nucleus after absorbing a neutron actually splits into two roughly equal pieces [Mei39]. This phenomenon came to be known as nuclear fission. *Meitner* and *Frisch* used a so-called liquid drop model of nuclei to describe the fission process by drawing on the similarity of the nuclear fission process with the division of a liquid sphere into two smaller droplets as a result of some deformation caused by an external disturbance. Soon after the discovery of the nuclear fission *Bohr* and *Wheeler* performed the first quantitative calculations based on the fission process using the liquid drop model [Boh39].

Nuclear Fission is characterized by the splitting of a heavy nucleus into two or more lighter nuclei. The resulting nuclei from fission are called fission fragments and usually denoted as FF. The most common and well known fission process is the binary fission. In binary fission a nucleus normally splits into only two lighter nuclear fragments. Physicists however soon realized that binary fission was not the only fission process that could result from the splitting of the nucleus and that the heavy nucleus could be split into three or more fragments. This resulted to the discovery of other nuclear fission processes namely ternary fission where nucleus splits into three fragments and quaternary fission, where the nucleus splits into four daughter nuclei. This thesis however will be devoted into the study of ternary fission with particular focus on collinear tri-partition.

## 1.2 Ternary Fission

Ternary fission was first discovered in 1946 by *Green L.L. and Liversy D.L.* [Gre47]. As already mentioned above, ternary fission is a process where a nucleus splits into two fission fragments accompanied by a light charged particle (LCP) which is usually an alpha particle. It is a consequence of the binary fission process where the fissioning nucleus splits into three fragments instead of the normal two. In instances where the nucleus splits into three particles of equal mass the process is known as *true ternary fission*. At the moment, there are two types of ternary decay of low and middle excited nuclei found to exist, namely *conventional ternary fission* and *polar emission* [Tsi47].

### 1.2.1 Conventional Ternary Fission

In a conventional ternary fission (usually just called ternary fission) a LCP which accompany the fission process is emitted almost perpendicular to the fission axis due to the strong focusing effect of the Coulomb field. The characteristics of these particles are influenced by the Coulomb field. Mostly *He* isotope is emitted, although particles up to the mass of 36 have been observed [Gon00].

This form of fission was intensively studied in experiments dedicated to spontaneous and thermal neutron induced fission. It was discovered that for the range of spontaneously fissioning or fissile actinides from Thorium to Fermium, the probability ratio of ternary to binary fission increases by a factor of about 5 [Gon04]. For the heavier ternary particles the yield depends on the fissioning compound. The fact that the LCP in the conventional ternary decay is emitted almost perpendicular to the fission axis demonstrates that the LCP is born near scission in the neck region of the two main fragments [Gon04]. By scission here we mean an instance of splitting of a nucleus.

Work carried out by *Ronen* on the study of *The Relationship between ternary fission and cluster decay* proved that the similarity between ternary fission and cluster decay suggest that other ternary emission can be considered to be cluster decays, just as ternary alpha emission may be seen as alpha decay [Ron02]. Cluster decay is generally defined as a radioactive decay in which the emitted particle is heavier than alpha particle (cluster decay will be discussed in more details later in this chapter). *Ronen* also suggested that the clusters obtained in cluster radioactivity, are related to clusters with high yield obtained in ternary fission. This suggests that ternary fission is a cluster decay of the fissioning nucleus in the last phase of the scission process.

Ternary fission is energetically more favorable than binary fission. Evidence of this was shown by *Swiatecki* [Swi58] on the calculations of the amount of energy released when a nucleus disintegrate into  $n$  fragments based on the liquid drop model. The results showed that fissioning of a heavy nucleus into three fragments releases more energy than binary fission for all nuclei with fission parameter  $30.5 < Z^2/A < 43.3$ . Swiatecki suggested that for the purpose of experimental detection of ternary fission one should use nuclei with maximum available value of fission parameter  $Z^2/A$ .

## 1.2.2 Polar Emission

Polar emission was first observed by *Piasecki* and his colleagues on their work on *Polar Emission and Evaporation from Fission Fragments* [Pia70] as an emission of charged particles moving almost along the fission axis. Polar emission was understood to be explained by a model based on a hypothesis that polar particles are evaporated from excited fission

fragments and this model was called *evaporation model* [Pia73], [Pia74]. At that time, this was the only model that could explain polar emission and attempts to verify this model were performed by comparing theoretical predictions with experimental data [Now82].

In the experiment presented in [Now82] where polar emission was investigated in  $^{252}\text{Cf}$  and  $^{235}\text{U} + n_{th}$  fission, about 4000 polar events were registered and identified. The intensity of polar emission was calculated by setting borderlines at  $15^\circ$  and  $155^\circ$  (the angles were measured with respect to the light fragment trajectory). In this way, it was possible to obtain the ratios of the polar to equatorial ( $P/E$ ) emission intensities for protons, deuterons, tritons,  $^4\text{He}$  and  $^6\text{He}$ . Knowing the  $P/E$  values one can determine the probability of polar emission. Comparison of the probabilities of polar emission in californium and uranium gave interesting results as discussed in [Now82]. It is worth noting that the  $P/E$  ratios decrease with increasing particle mass and a similar dependence was also observed in the case of  $^{236}\text{U}$  presented in [Pia80].

The energy of a polar particle is higher than the energy of particles emitted in the conventional tri-partition. Although it seems that this energy changes smoothly on passing from equatorial to polar range of angles. The kinetic energy of fission fragments which are accompanied by polar particles is lower than in bi-partition. The decrease of the energy of the fission fragments which moves in the same direction as the polar particle is explained by the recoil effect due to the particle emission. A similar decrease of energy for the fission fragment moving in the opposite direction to the polar particle is also observed. This means that polar emission prefers more stretched scission configurations as compared to conventional binary fission.

The mass distributions of  $^{252}\text{Cf}$  fission fragments moving in the same direction as polar particles are presented in Fig 1.1 below. If the polar emission along the light fragment trajectory is considered the L-emission and along the heavy fragment trajectory the H-emission then the asymmetry of the distributions shown in Fig 1.1 reflects the differences between the intensities of L-emission and H-emission, that is, the fact that the polar emission along the light fragment trajectory is more frequent than along the heavy fragment.

It is not known, whether the polar emission is a sequential process of binary fission which is followed after some delay by the light particle emission, or whether it is a three body-break

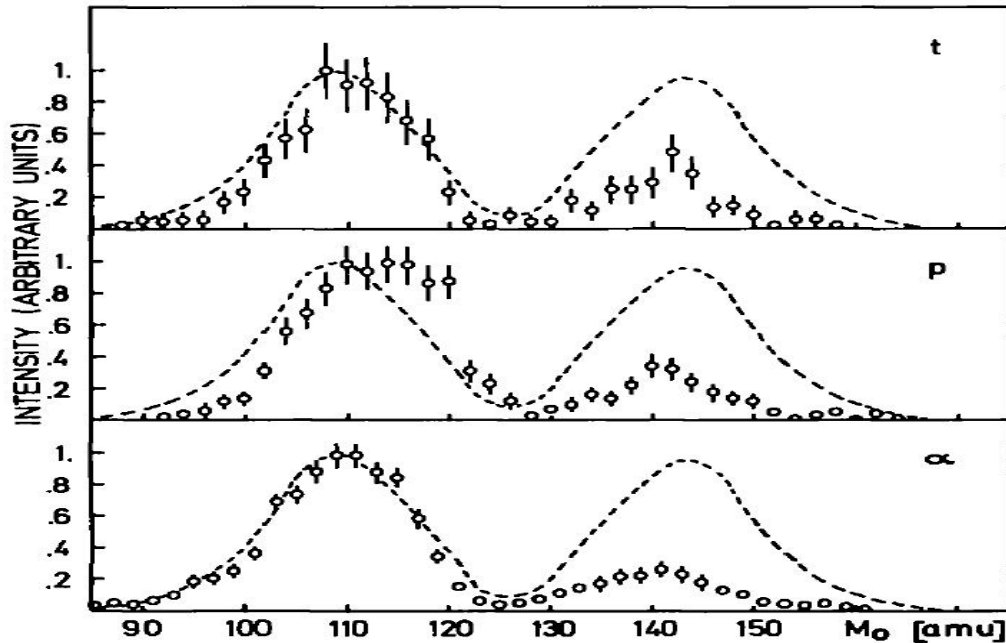


FIG. 1.1. Mass distribution of  $^{252}\text{Cf}$  fission fragments obtained from [Now82].

up process. If the process is a sequential one and the delay is greater than, say  $2 \times 10^{-21}\text{s}$ , then it is highly probable that the emission takes place from the fragment going in the same direction as the emitted light particle [Pia75]. This is because; in the other case the initial energy of this particle would be unreasonably high to overbalance the fragment velocity and to give finally the observed  $23\text{MeV}$  of kinetic energy in the lab system [Pia75].

### 1.2.3 True Ternary Fission

True ternary fission as already defined above, is the disintegration of a nuclear system into three fragments of comparable masses. It was also mentioned that this process is not only energetically permitted but is also more favorable than binary fission [Pre41].

Fission of a nucleus into three fragments of equal mass is a rare event as concluded by *Perfilov et al* in their work of *Physics of Nuclear Fission* [Per57], [Mug63], [Sto66]. The presence of true ternary decay was declared by *Muga et al* in their study of *Ternary Fission of Heavy Nuclei* [Mug67] from the series of experiments on actinide targets to have a yield of about  $10^{-6}$  per binary fission.

According to the results of instrumental measurements, when uranium is bombarded by slow neutrons, only one ternary fission is observed for every  $10^5 - 10^6$  binary fission. When the energy of the bombarding particle is increased, the probability of fission into three fragments of equal mass was observed to be increasing [Fle66], [Iye66].

### 1.3 Collinear Cluster Tri-partition

The fission process where by a nucleus disintegrate into three particles is bounded by two extreme modes. One mode is where the scission neutron is accompanied by two primary fragments and the other mode is the production of three primary fragments with approximately equal masses. The given definition of *ternary fission* covers the whole spectrum of the two extreme mode boundaries. The mode where three fragments of approximately equal masses are emitted is referred to as true ternary fission. In cases where the nucleus disintegrates into three fragments and the fragment mass ratio and the other parameters of fission can be ignored, the fission process is referred to as tri-partition.

Calculations of equilibrium shapes of the fissioning nucleus performed by *Strutinsky* in the liquid drop model (see Fig 1.2) [Str63] showed that along with the ordinary configuration in a scission point of a nucleus with one neck, there is a possibility of having even more elongated complicated configurations with two or three necks even though such configurations are less likely to happen. *Diehl* and *Greiner* also showed that fission of a nucleus into three fragments of similar size prefers a prolate over the oblate saddle point shape [Die73], [Die74]. Such pre-scission configurations could lead to an almost collinear separation of decay partners at least in a sequential fission process [Pya10].

In our previous experiments, strong indications of ternary fission with almost collinear kinematics of the products and clustering as a physical reason of the process were observed. The total mass of the two registered fission fragments which fly apart almost collinearly was significantly less than the mass of the initial nucleus. The mass of at least one of the detected fragments corresponded to the mass of one of the known magic nucleus. This decay channel is referred to as “*Collinear Cluster Tri-partition (CCT)*”.

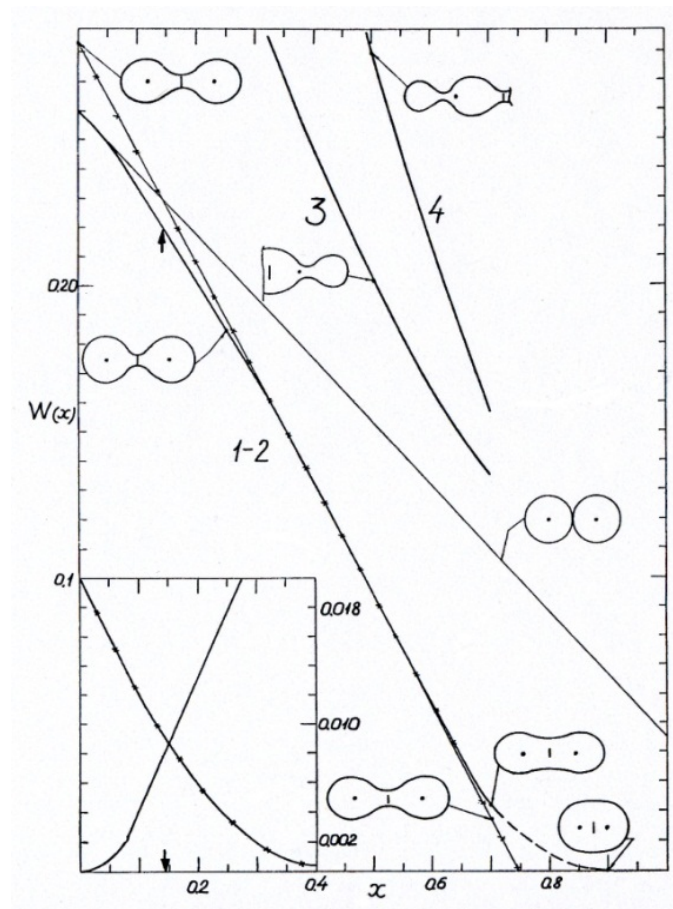


FIG. 1.2. The potential energy of absolute equilibrium shapes for the conventional sequence of shapes (1 and 2), two-neck shapes (3) and three-neck shapes (4) [Str63].

### 1.3.1 Experimental Evidence of the Collinear Cluster Tri-partition

The Flerov Laboratory of Nuclear Reaction (FLNR) of the Joint Institute for Nuclear Research (JINR) in Russia has in the past performed a number of experiments devoted to the search for collinear cluster tri-partition (CCT). One of the experiments where the CCT was revealed for the  $^{252}\text{Cf}$  nucleus is discussed below.

The CCT manifested itself via pronounced structures in the mass-mass distribution of the fission fragments. There are a number of methods that can be used to measure the mass of nuclear reaction products and these methods include the double energy versus double velocity ( $2E - 2V$ ) method, the double energy ( $2E$ ) method, the double velocity ( $2V$ ) method, etc [Kim93]. The  $TOF - E$  (time-of-flight versus energy) method however is the only one that uniquely allows the study of the multi-body decays. The method allows the measurement of both the velocity  $V$  of the fragment obtained from the  $TOF$  and the energy  $E$  for each fragment individually. The fragment mass  $M$  is calculated by simply using the kinematic equation  $M = 2E/V^2$ .

The experiment (see Fig 1.5) to be discussed here was performed with the Modified FOBOS Spectrometer setup at the Flerov Laboratory. The Modified FOBOS setup is a two-arm spectrometer setup. Each arm consists of five big and one small standard FOBOS modules [Ort98]. Each module includes a position-sensitive avalanche counter (PSAC) and a Bragg ionization chamber (BIC). Such a double-armed TOF-E (time-of-flight vs energy) spectrometer allows a measurement of the energy and the velocity vectors of the coincident fragments. The scheme of the modified FOBOS setup and the overall view of the original FOBOS setup are shown in Fig 1.3 and Fig 1.4 respectively.

About  $13 \times 10^6$  coincident binary events were recorded for this experiment. The  $TOF$  of the fragments was measured over a flight path of  $50\text{cm}$  between the “start” detector (indicated by 3 in Fig 1.5) which is also referred to as the Micro-Channel Plate (MCP) based detector. The detector is placed next to the  $^{252}\text{Cf}$  source (1) and the “stop” Position Sensitive Avalanche Counter (PSAC, 4).

The energies of the coincident fragments that pass through the PSACs were measured in



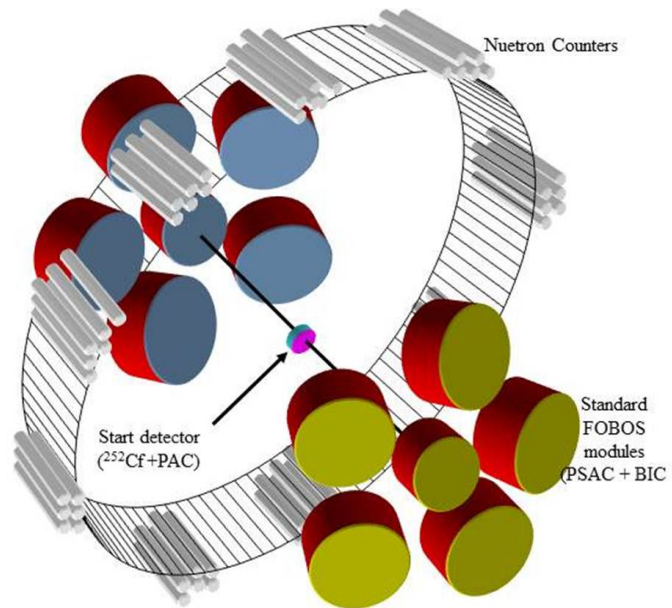


FIG. 1.3. Schematic view of the modified FOBOS setup.

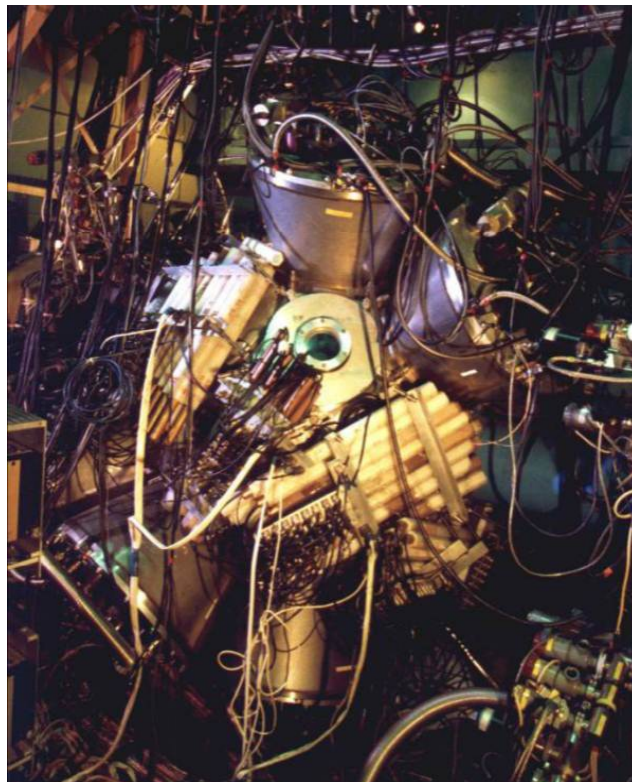


FIG. 1.4. The overall view of FOBOS spectrometer with a belt of neutron counters.

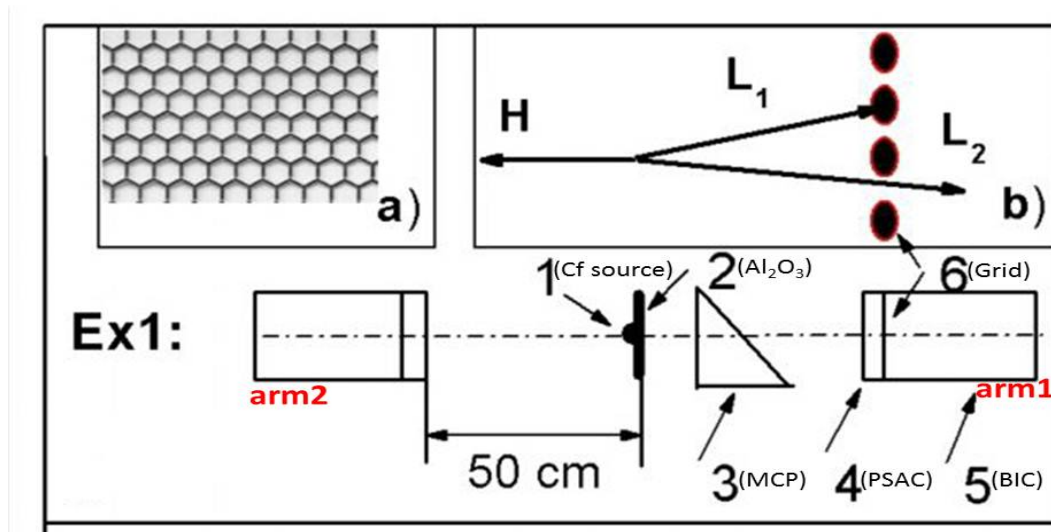


FIG. 1.5. A scheme of the experiment performed at the FOBOS setup for coincidence measurement of two fragments of the CCT partners for  $^{252}\text{Cf}$  [Pya10].

the Bragg Ionization Chamber (BIC, 5) with entrance window supported by a grid (6) that has a transparency of 75%. The geometric structure of the grid is hexagonal as shown in insert (a) of Fig 1.5. The  $^{252}\text{Cf}$  source is mounted on  $\text{Al}_2\text{O}_3$  backing (2) of thickness  $50\mu\text{g}/\text{cm}^2$ , while the other side is free or coated with  $\text{Au}$  of  $20\mu\text{g}/\text{cm}^2$ .

## Results

A detailed explanation of the results obtained in the above experiments is presented in [Pya07a], but it is worth highlighting the salient points of the results that revealed the CCT decay. A two dimensional distribution of the two registered masses of the coincident fragments in the experiment at the FOBOS setup is shown in Fig 1.6 below.

The outstanding structures seen from the above distribution are the “tails” marked by the numbers 3 to 7. The structures marked by number 1 and 2 show fragments from the conventional binary fission. The interesting events are separated from the normal binary fission events by a line that represents the total mass of  $M_{total} = 225$ . The “tails” marked

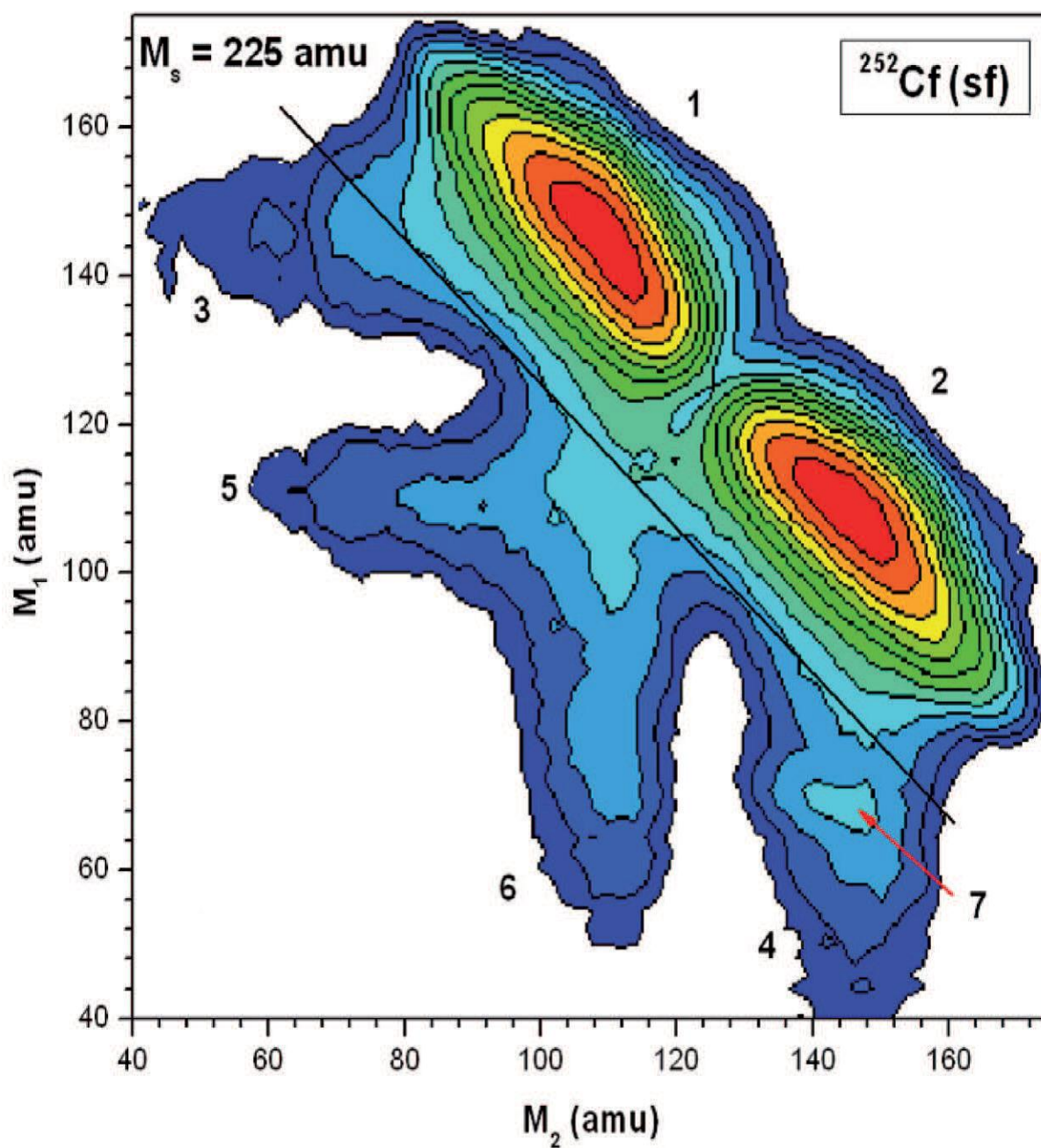


FIG. 1.6. Contour map of the mass-mass distribution of the collinear fragments detected in coincidence in the two opposite arms of the FOBOS spectrometer setup [Pya10].

by the numbers 3 to 6 are mainly due to the scattering of the fragments on the foil and the grid of the “stop” detectors. There is a difference between “tail” 3 and “tail” 4 which is the distinct structure or “bump” that is marked by number 7 and is oriented approximately parallel to the line that defines the constant sum of the detected masses.

This astonishing “bump” (structure number 7 in Fig 1.6) is located in the region that corresponds to a large “missing mass”. This “bump” can be explained by considering insert (b) shown in Fig 1.5. One must also take note of the fact that when the ternary fission takes place the two light fragments are emitted in the same direction with the third heavy fragment being emitted in the opposite direction. The two light fragments going in the same direction are separated by an angle which is less than  $1^\circ$  after passing through the backing of the source. The backing of the source is located on the side of tail 4.

In the case that both light fragments (i.e the two going in the same direction) pass through the hexagonal grid and enter the BIC, a signal corresponding to the sum of the energies of the two fragments is registered as a binary fission event. In the other case, when one light fragment passes through and enter the BIC, while the other light fragment is stopped (lost) in the supporting grid of the ionization chamber, then only a proper energy (or mass) of one light fragment is registered. This methodic approach is called the “missing mass” method, because the mass of one of the light fragments is lost.

## Discussion

The experimental observation from this experiment was interpreted as a collinear ternary decay with two fragments of similar mass and one heavy fragment [Pya10]. This result was different from the previously reported ternary fission [Gon05], where a third light fragment was emitted perpendicular to the axis spanned by the heavy fission fragments.

The distribution which shows a contour map of ternary mass splits is shown in Fig 1.7. This distribution is free from experimental background and binary fission events. As mentioned above, the ternary process that is being considered here is the one where one heavier fragment and two light fragments are emitted.

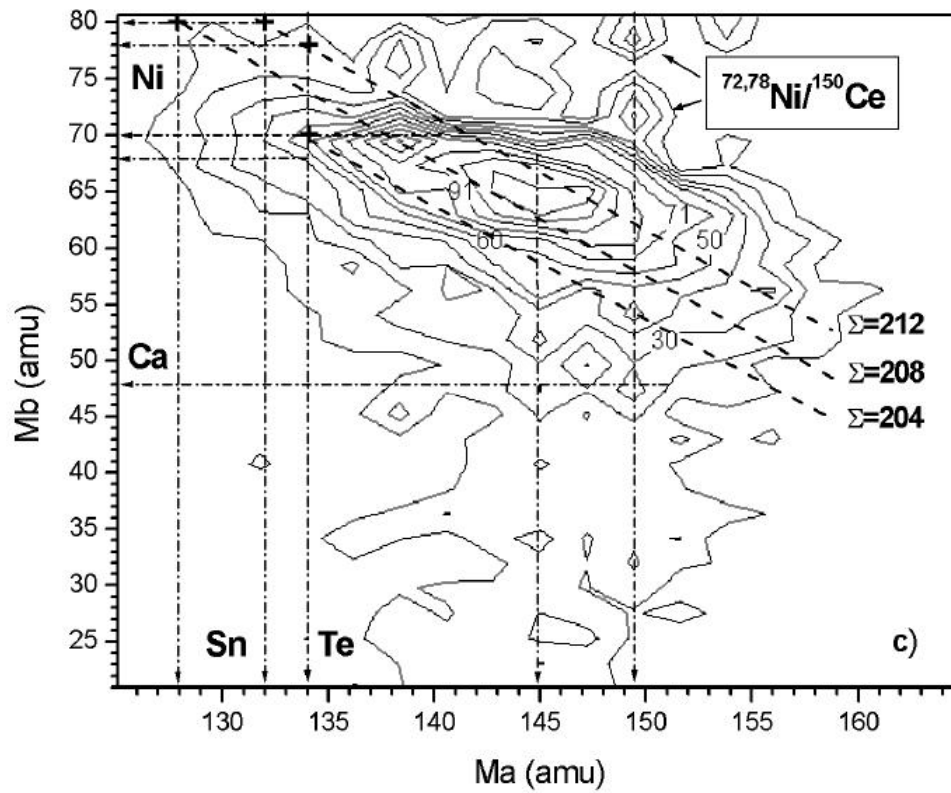


FIG. 1.7. Distribution which shows a contour map of the difference between the tails 3 and 4 in Fig 1.6

As can be seen in Fig 1.7, the ridges (marked by the dash lines) pass through crossing points corresponding to different combinations of two fragments with “magic” nucleon numbers (marked by the dot-and-dash arrows). These marked points are related to mass values with magic subsystems that are well-known from binary fission [Wil76], [Roc04]. These magic subsystems are:

$$\begin{aligned}
 &204 \rightarrow {}^{70}\text{Ni} + {}^{134}\text{Te} \text{ or } {}^{72}\text{Ni} + {}^{132}\text{Sn} \text{ missing } {}^{40}\text{Ca} \\
 &208 \rightarrow {}^{80}\text{Ge} + {}^{128}\text{Sn} \text{ missing } {}^{44}\text{S}_{28} \\
 \text{For } M_{total} = 212 &\rightarrow {}^{80}\text{Ge} + {}^{132}\text{Sn} \text{ or } {}^{78}\text{Ni} + {}^{134}\text{Te} \text{ or } {}^{68}\text{Ni} + {}^{144}\text{Ba}
 \end{aligned}$$

It should be stressed that the observation of the structures for the masses of the emitted fragments and the “missing” masses corresponding to the known shells must be seen as conclusive argument in favor of the physical origin of the effect of tri-partition [Pya07a]. Some features of the two dimensional distribution shown in Fig 1.7 above can be further emphasized by applying a second derivative filter to Fig 1.7. The result of this process is shown in Fig 1.8 below. The second derivative filter is typically used in the search for gamma spectra and further details on it can be found in [Mar67] and [Pya02]. As can be seen in Fig 1.8 the maxima of the peaks extend over certain linear regions of  $M_2 = \text{constant}$ , which are found predominantly as discrete diagonal lines. These lines correspond to the total masses  $M_2 = \text{constant}$  with values of 204, 208, 212 and perhaps 214amu, respectively.

One of the decay modes which contribute to the bump discussed above can be treated as a new type of cluster decay as compared to the well-known heavy ion or lead radioactivity [Pya10]. The relatively high CCT yield can be understood if one assumes collective motion through the hyper-deformed pre-scission shapes of the mother systems, which is supported by the fact that the linear arrangement recognizes the lowest Coulomb potential energies of three clusters. It should also be emphasized that the Q-value for ternary fission is 25 – 30MeV more positive than in binary fission, due to the formation of magic fragments [Pya10]. Thus the ternary fission process must be considered to proceed sequentially with two neck ruptures in a short time sequence characteristic for binary fissions. The comparison between the parameters of the CCT and lead radioactivity is shown in Fig 1.9.

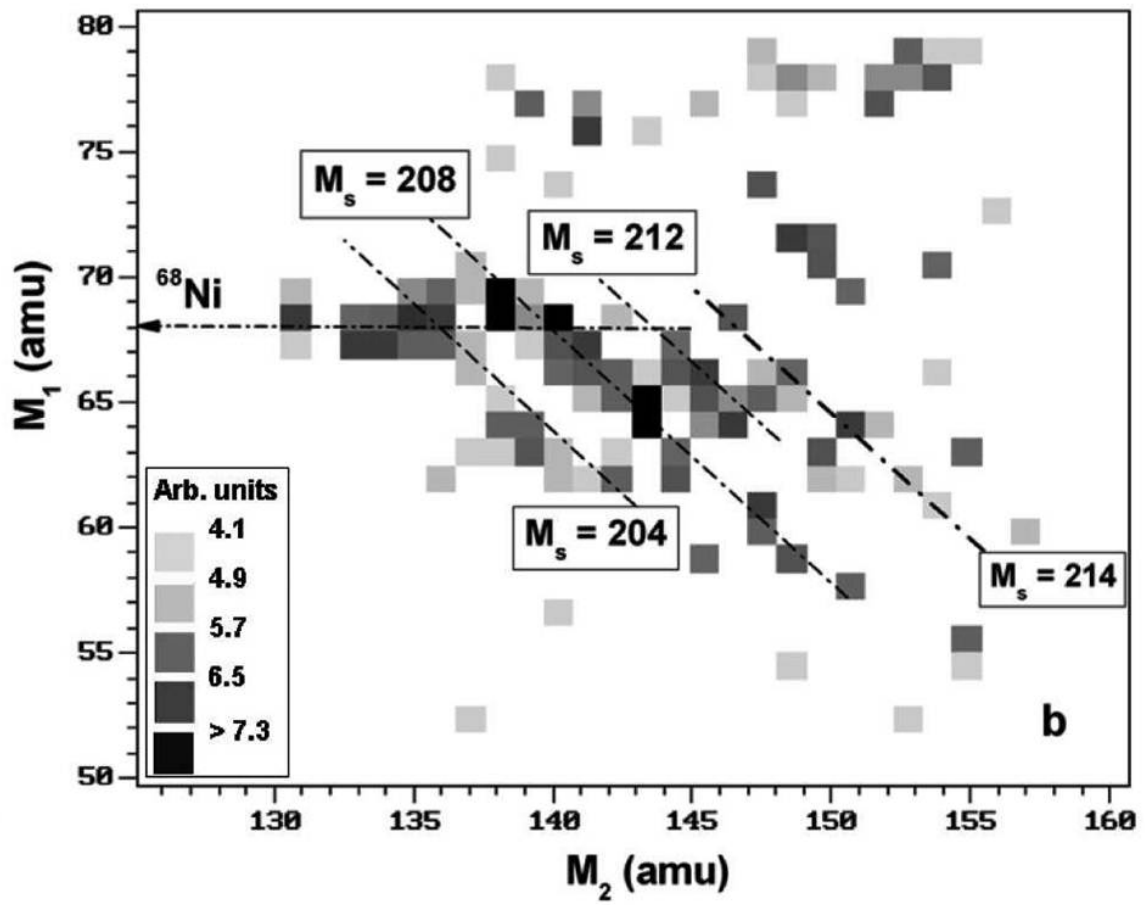


FIG. 1.8. Shows the same distribution as in Fig 1.7 but a second derivative filter has been applied to emphasize the local peaks in each section of the  $M_s = \text{constant}$ .

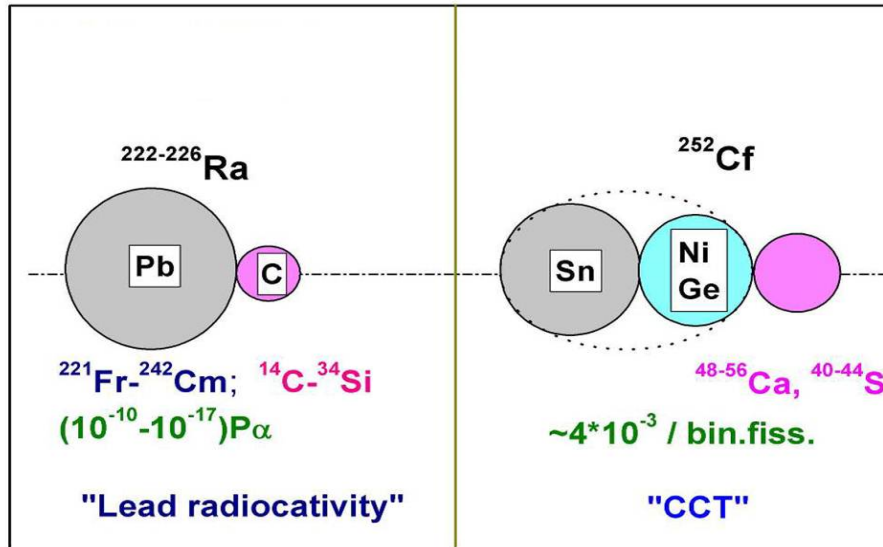


FIG. 1.9. Parameters of Lead Radioactivity in comparison with those of CCT [Pya10].

### 1.3.2 “Sn-lost” CCT mode

In an experiment performed with one of the collaborating partners at the Accelerator Laboratory of the University of Jyväskylä (JYFL) a specific CCT mode based on the lost double magic  $^{132}\text{Sn}$  cluster was observed. This mode was referred to as a “Sn-lost” CCT mode due to the fact that it was realized that the lost nucleus was the double magic  $^{132}\text{Sn}$ . Further description of this phenomenon is given below. The experiment which revealed this phenomenon required a special time-of-flight spectrometer which was installed in the Large Scattering Chamber facility at JYFL. The scheme of the experimental setup of this time-of-flight spectrometer is shown in Fig 1.10. In this setup a thin  $^{252}\text{Cf}$  source is placed in the middle of a symmetric setup with a total of 4 Micro-Channel Plate (MCP) based detectors and two PIN diodes.

Each arm of the spectrometer setup consists of two MCP detectors. The separation distance between the MCP detectors is  $8\text{cm}$  with the first MCP  $6\text{cm}$  from the source. The total flight-path for fission fragments from the source to the PIN diode is  $21\text{cm}$ . The MCP detectors provided time-of-flight signals with resolution of approximately  $120\text{ps}$ . This setup provided a total of eight parameters, four more than the standard FOBOS setup which made it possible to perform additional crosschecks for data consistency.



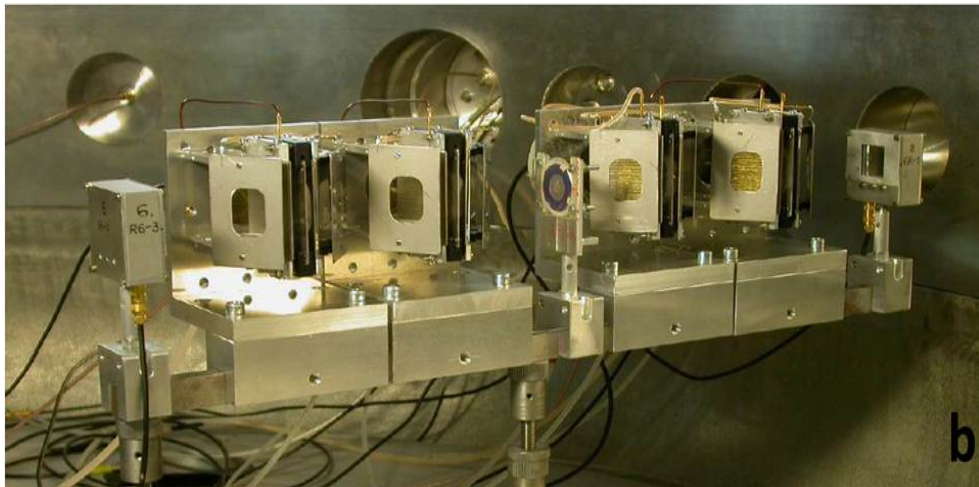
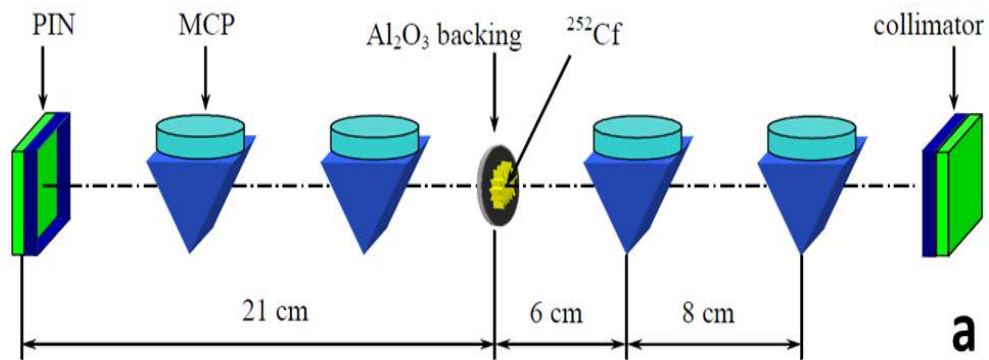


FIG. 1.10. A scheme (a) and a photo (b) of the setup performed at JYFL.

## Results and Discussion

From this experiment a specific mode based on the double magic  $^{132}\text{Sn}$  cluster was observed. The mass-mass distribution of the events selected by velocities and energies of this mode is shown in Fig 1.11.

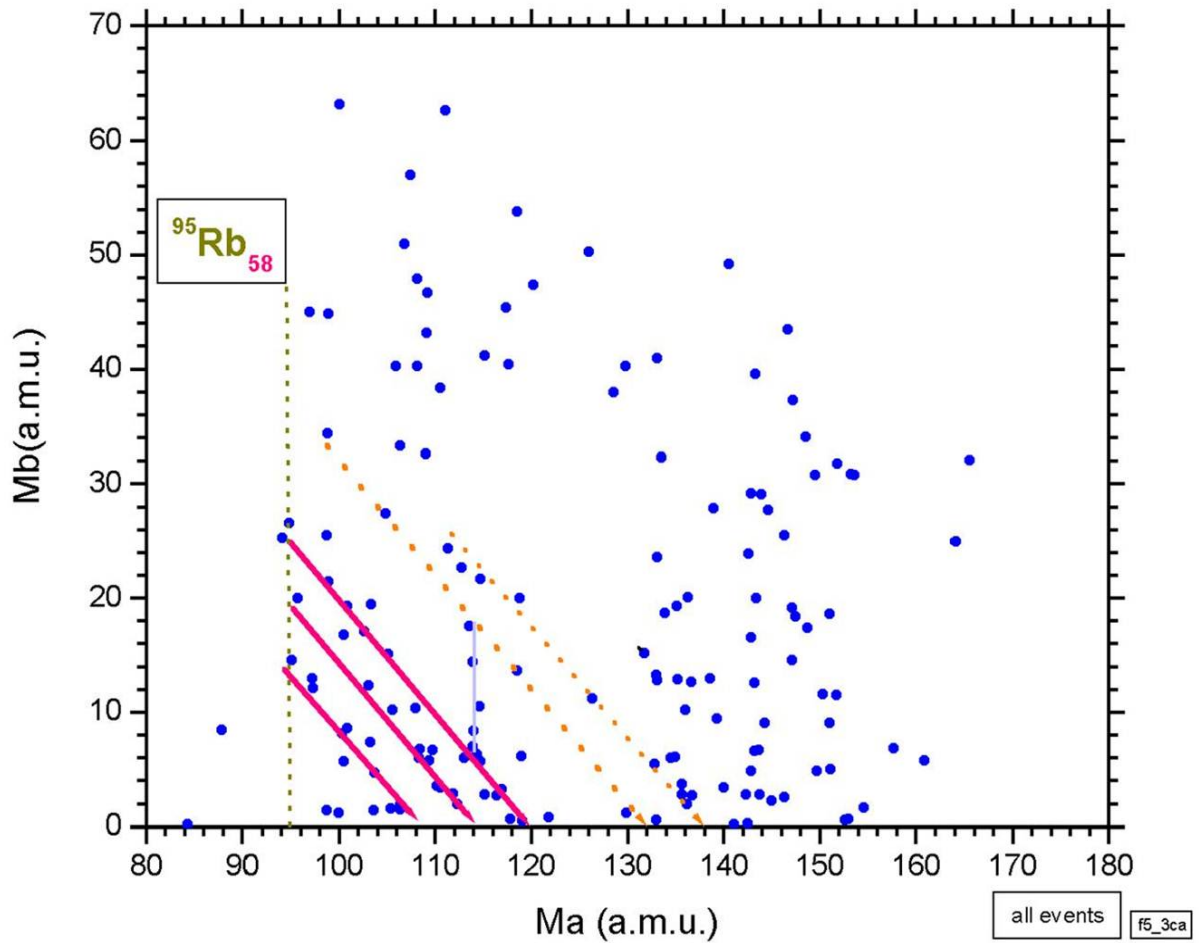


FIG. 1.11. Mass-mass distribution of fragments selected by velocities and energies for the “Sn-lost” CCT mode.

The tilted lines in Fig 1.11 correspond to the missing magic clusters of  $^{132}\text{Sn}$  and  $^{144}\text{Ba}$ . This missing cluster can be clearly seen in the mass spectrum in Fig 1.12 which is the projection along these lines. Pre-scission configuration which presumably gives rise to the mode under discussion is shown in Fig 1.13. As we can see from Fig 1.13, the  $\text{Sn}$  cluster can

“move” as a whole along the cylinder-like configuration that consists of residual nucleons. Two light fragments accompanying this cluster marked by  $M1$  and  $M2$  were actually detected in previous experiments. The value of  $M2$  lies between  $0amu$  and the difference between the initial mass of  $^{252}Cf$  and the detected fragments.  $M1$  cannot assume any value less than  $95amu$  (deformed magic  $^{95}Rb$ ).

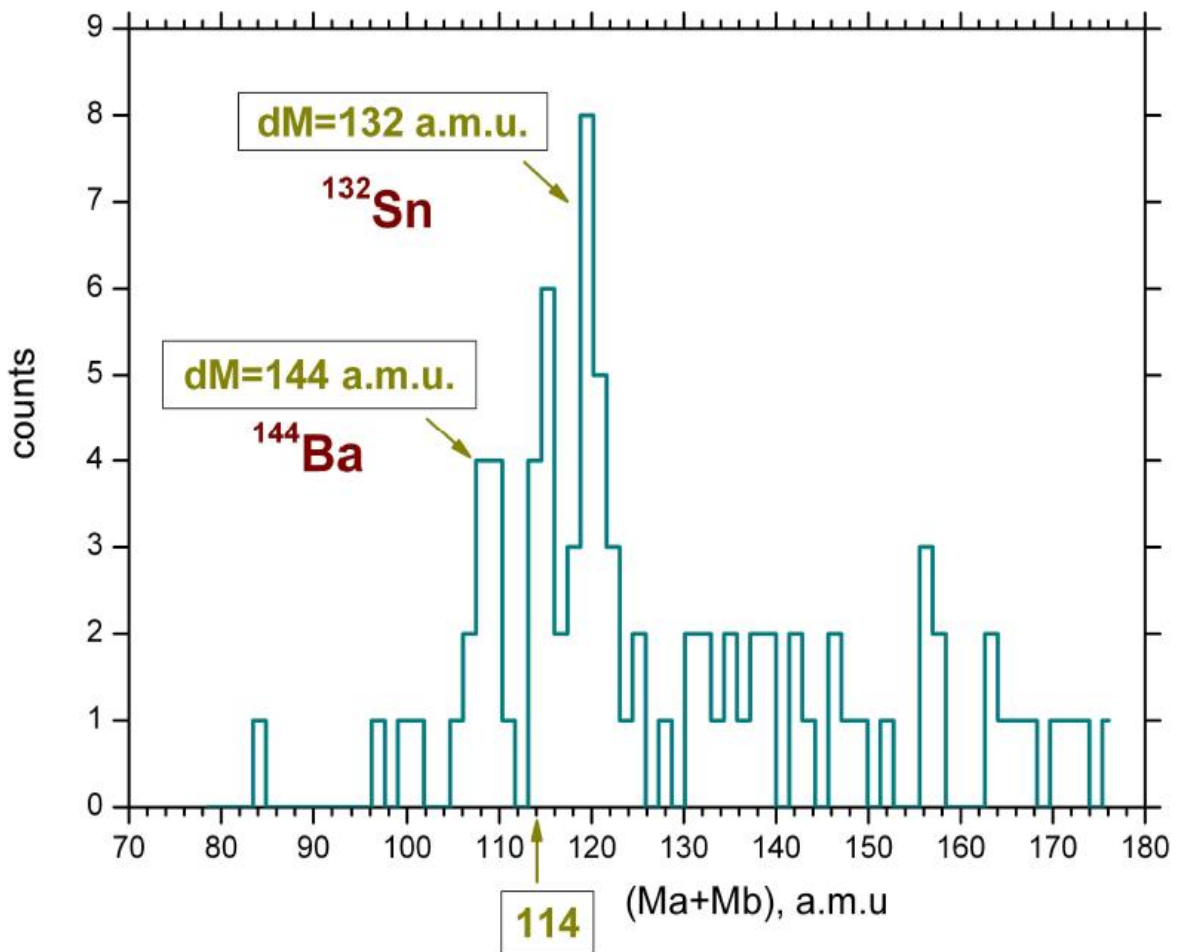


FIG. 1.12. Mass spectrum for the structures marked by red lines in Fig 1.11

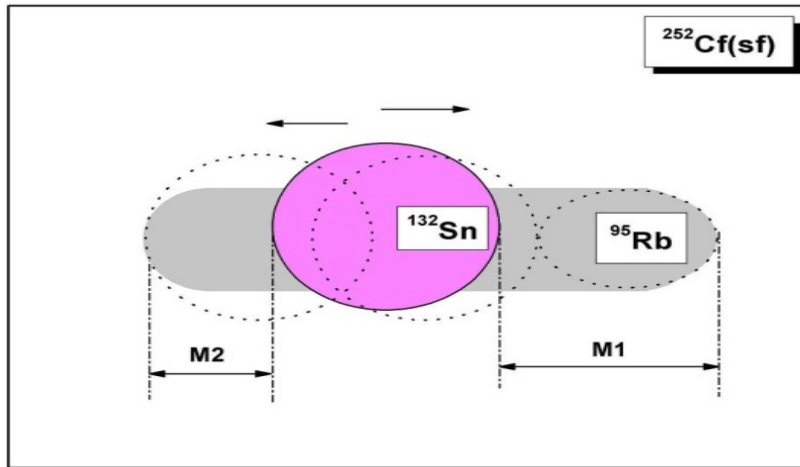


FIG. 1.13. Schematic pre-scission configuration of the CCT mode based on the double magic  $^{132}\text{Sn}$  cluster.

### Motivation for the development of the new setup

The question that arises here is whether  $^{132}\text{Sn}$  can be replaced by the double magic  $^{208}\text{Pb}$  in this decay mode. Theoretical indications of such a mode were obtained in [Pas09] and are shown in Fig 1.14. As the figure shows the potential energy of the fissioning nucleus of  $^{252}\text{Cf}$  corresponds to the bottoms of the potential energy valleys as a function of parameter  $Q$  ( $Q$  is proportional to the quadrupole moment of the system).

Compact shapes of the system along the valley of lead radioactivity, marked by 1 in Fig 1.14 give rise to the huge barrier in this channel which gives a very low decay yield. This is in sharp contrast to the elongated pre-scission chain-like configuration in the CCT channel which provides the dramatic decrease of the barrier resulting in a high CCT yield [Pya10a].

The relatively high CCT yield can be understood by assuming a collective motion of the hyper-deformed pre-scission shapes of the mother systems, which is supported by the fact that the linear arrangement recognizes the lowest Coulomb potential energy of the three clusters. It should also be emphasized that the  $Q$ -values for ternary fission are 25 – 30 MeV more positive than in binary fission, due to the formation of magic fragments [Pya10]. Thus the ternary fission process must be considered to proceed sequentially with two neck ruptures in a short time sequence characteristic for binary fissions.

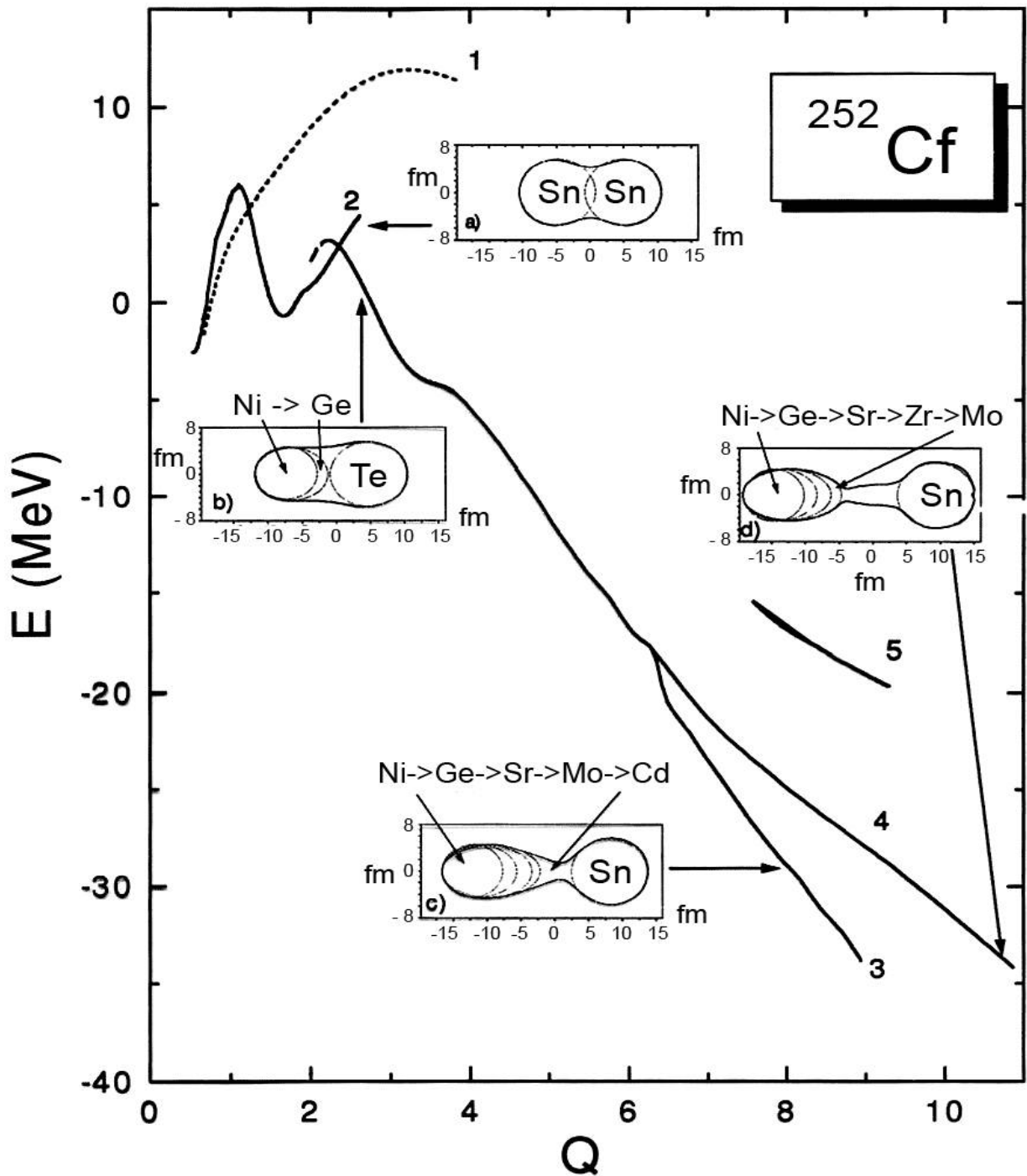


FIG. 1.14. Potential energy of the fissioning nucleus of  $^{252}\text{Cf}$  corresponding to the bottom of the potential valleys as a function of a parameter  $Q$  proportional to the quadrupole moment [Pya10a].

Considering the possibility that  $^{132}\text{Sn}$  can be replaced by double magic  $^{208}\text{Pb}$  opens up a new mode of lead radioactivity. Searching for such a mode is one of the goals for designing a Light Ions Spectrometer which will produce better statistics and more precise time-of-flights measurements.

## 1.4 Conclusion

The results of the experiments presented above were obtained in the framework of the “missing mass” approach meaning; only two fragments were actually detected with the third one missing. The total mass of the detected fragment being less than the mass of the mother system serves as an indication of the multi-body decay. The direct detection of all the decay products will provide the most convincing experimental approach. However direct detection of all the decay partners presents its own set of complications as one need to use a mosaic detection system.

A multi-detector registration system for the study of multi-body decays of heavy nuclei is needed to achieve the direct detection of all the decay partners of the proposed decay scenario. Chapter two of this thesis will give a description of the experimental techniques where two multi-detector registration systems are presented. The first detector system to be discussed is called the Correlational Mosaics E-T Array (COMETA) setup. The so called “Neutron Belt” of the COMETA setup, the electronics and data acquisition system will be discussed in the same chapter. A description of the second and latest setup in the detection of multi-body decay referred to as Light Ions Spectrometer (LIS) will also be the focus of chapter 2. Physical motivation and the electronics of LIS will also be discussed. Both LIS and COMETA setup use similar data acquisition system.

Data analysis will be presented in chapter three. In this chapter calculation of the detection efficiency of the “Neutron belt” of the COMETA setup using both results obtained from a modeling process and experimental data will be discussed. Stability of the data and calibration process for the two detector systems will also be discussed. Plasma delay and correctness of velocity measurement will also be discussed in this chapter and lastly the first data obtained from the LIS setup will be analyzed.

Chapter four will focus on preliminary results of the LIS setup and conclusions for future experiments. This chapter will also provide a conclusive summary of all the work covered and provide plans for the future experiments.

# Chapter 2

## Experimental Setups and Techniques

### 2.1 Introduction

In this chapter, the focus is on the various techniques and systems used in the detection and investigation of Collinear Cluster Tripartition (CCT). In the previous studies of this rare decay phenomenon most of the experimental observations were undertaken under the “missing mass” method, i.e. only two out of the three fragments were detected the other one was missing (as was discussed in chapter 1). To further understand this phenomenon very well, different nuclear systems in a wide range of excitations were investigated. From all the methods followed, it became evidently clear that direct detection of all three decay partners would prove to be a more convincing experimental approach compared to the “missing mass” method. Therefore a far more complex spectrometer of high granularity capable of detecting all decay partners was needed.

A simpler prototype of such a spectrometer was successfully used in an earlier experiment at the Flerov laboratory. With this prototype all decaying partners from the ternary fission of  $^{234}\text{Pa}$  from the reaction  $^{232}\text{Th} + d(10\text{MeV})$  were observed [Kam10a]. The yield of this effect was dependent on the geometry of the experiment and amounted to  $10^{-5}$  per binary fission. The experimental angular spread of the ternary decay products flying in the same direction was observed to range from  $1^\circ$  up to  $20^\circ$  [Kam10a]. The mass spectrum of the lightest fragment from each detected triplet of fragments revealed a gross peak in the range of  $20 - 40\text{amu}$ . The spectrum agreed with the results from our CCT studies under



the missing mass method [Pya07a], [Kam08].

## 2.2 Overview of the Si Detector Based Mosaic Spectrometers

Technological advances in semiconductor technology allowed experimentalist at Technische Universitat Munchen in Garching Germany to build a first so called double-arm fission fragment spectrometer. The very first successful double-arm spectrometer with large PIN diode detector array (Mosaic) was reported by *Kim Y.S. et al* [Kim93]. Before the development of such technology silicon surface barrier (SSB) detectors were used for spectrometric experiments because of their very thin dead layer, which is a quality that is essential for the detection of heavy fragments.

The use of semiconductor detectors as double arm spectrometers in fission spectroscopy however brings about two technical challenges. The first challenge is the correction of pulse height defect (PHD) which refers to the difference between the energy of a heavy ion and that of an alpha particle yielding the same pulse height [Yam07] and has serious effect on the data. The accuracy of the data is directly limited by the accuracy of the PHD correction. The second challenge is “plasma delay”. The “plasma delay” however has less effect on the data than the PHD and can be reduced by increasing the flight length. Various PHD correction schemes developed for the use of semiconductor detectors were mutually consistent only within a few  $MeV$  which was not satisfactory for the purpose of the current experimental studies.

## 2.3 Motivation for using Mosaic Spectrometers in the study of the CCT phenomena.

Understanding the CCT process in details will require much more effort in both theory and experiments. However from the observations and results obtained from previous experiments [Pya07a], [Pya10] and [Pya10a]; one can draw reliable conclusions regarding the existence of the CCT process. The observed ternary decay has been considered as a

sequence of two neck ruptures of a hyper-deformed shape. Following the neck ruptures, strongly deformed substructures are formed with their masses equal to the sum of two magic clusters (that consist of  $Sn$  or  $Te$  for heavy fragments and  $Ge$  or  $Ni$  for light ones) and a complementary light fragment  $L_1$  [Pya07a]. A next rupture of the heavy fragment from the first stage leads to a formation of a second light cluster  $L_2$  and a complimentary heavier fragment with a mass slightly larger than  $Sn$  or  $Te$ . An alternative case leading to the horizontal lines shown in Fig 1.7 of chapter 1 differs by a creation of  $Ni$  cluster at the first step of the process [Pya07a].

The results presented in chapter 1 and by [Pya07a] for the decay of  $^{252}Cf$  nucleus show that the true ternary spontaneous decay channel has been observed with good statistical accuracy and in agreement with the latest theoretical expectations [Poe02]. The decay fragments with masses in the vicinity of magic  $^{132}Sn$ ,  $^{70}Ni$  and  $^{48}Ca$  isotopes fly apart almost collinearly. The probability of this decay is not less than  $4 \times 10^{-3}$  relative to binary fission [Pya07a]. Thus the probability of this decay is larger than that of the known light charged particles accompanied “ternary fission”. From the evidence of the results provided above it is therefore clear that the decay is due to the formation of multi-component nuclear molecules based on magic nuclei as clustered substructures in the body of the decaying system.

The use of traditional spectrometers in the detection of CCT brings its own set of challenges. The masses defining the decay mode under investigation differ radically, that is, one is very light while the second one is very heavy. Therefore the challenge with the traditional spectrometric detector systems is to be able to measure the correct energy and time-of-flight of heavy ions in this wide range of energies and masses. For this reason it is therefore more advantageous to use a Mosaic Spectrometers in the study of CCT phenomena than the traditional spectrometric detector systems as it is explained in the follow-up section.

## 2.4 COMETA Setup

In order to increase the reliability of selecting the CCT events by means of direct detection of all the partners, a new mosaic of PIN-diodes spectrometer referred to as COMETA (Correlation Mosaics Energy-Time Array) spectrometer was brought into operation at the Flerov Laboratory.

### 2.4.1 Description of the COMETA setup

The COMETA is a double arm time-of-flight spectrometer that consists of a Micro-Channel Plate (MCP) based “start” detector, two mosaics of eight PIN diodes each and a “neutron belt”. The schematic view of the COMETA is shown in Fig 2.1 and the photographic view of the COMETA setup is shown in Fig 2.2.

The design of the MCP based “start” detector is in such a way that the  $^{252}\text{Cf}$  source is installed inside the detector. The size of each PIN diode in each mosaic is  $2\text{cm} \times 2\text{cm}$  and provides both the energy and time signals. The “neutron belt” which comprises of 28  $^3\text{He}$  filled neutron counters is located in the plane perpendicular to the symmetry axis of the setup. The distance between the MCP based “start” detector and the mosaics in each arm is  $15\text{cm}$ .

### 2.4.2 “Neutron belt” of the COMETA

The COMETA setup as shown in Fig 2.1 and Fig 2.2 consists of 28  $^3\text{He}$  filled neutron counters that are positioned as a belt around the start detector of the spectrometer and used for the detection of neutrons in coincidence with the fission events. When a fission event is registered by the mosaics or PIN diodes, it triggers the neutron counters to open a gate for the detection of neutrons.

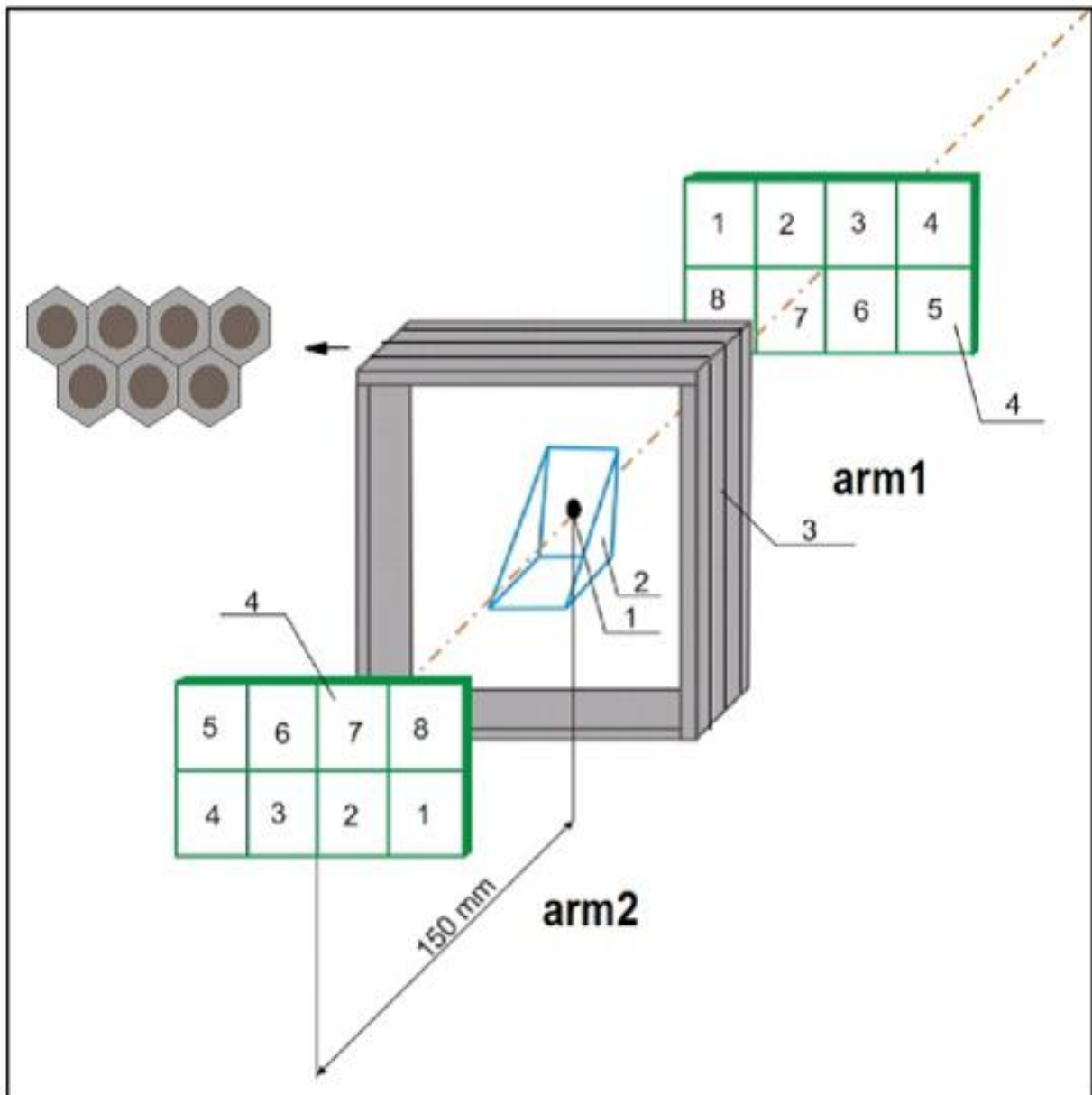


FIG. 2.1. Scheme of the COMETA which consist of two mosaics of PIN-diodes (4), MCP based “start” detector (2) with  $^{252}\text{Cf}$  inside (1) and a “neutron belt” (3) that consist of 28  $^3\text{He}$ -filled neutron counters. The configuration of the belt is shown on the insert marked by the arrow.

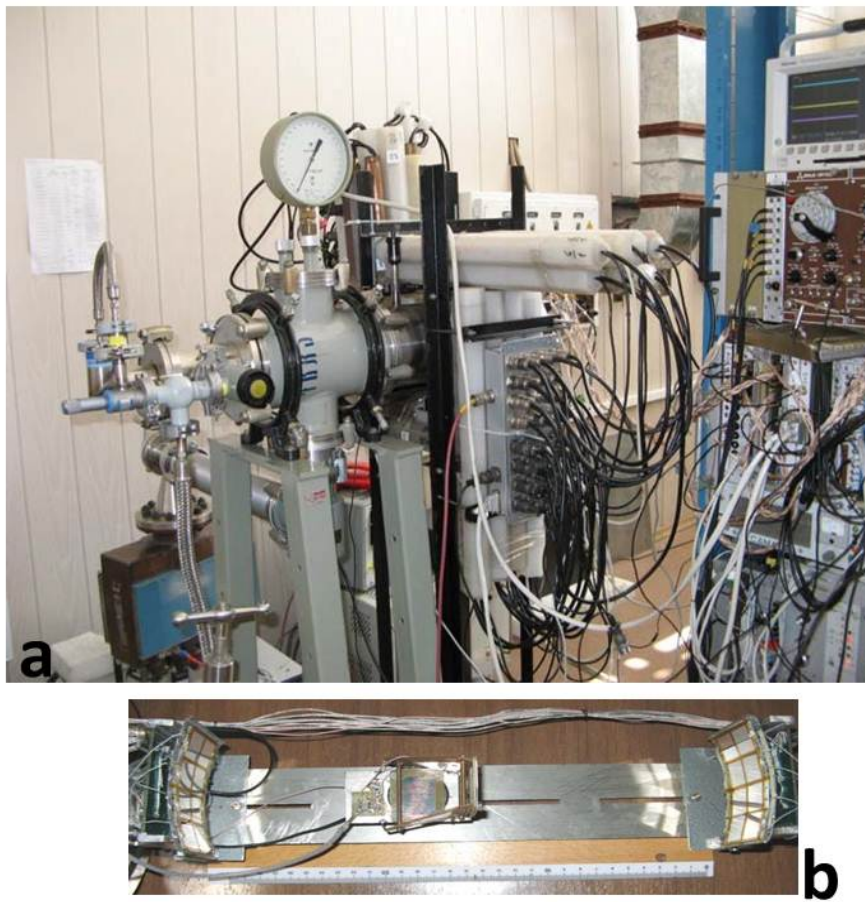


FIG. 2.2. a) Overall view of the COMETA and the “neutron belt” b) MCP “start” detector and mosaics of PIN diodes mosaic.

## Neutron Counters

As it is describe above the “neutron belt” used in the detection of neutrons in coincidence with the fission fragments consist of 28  $^3\text{He}$  neutron counters. Each neutron counter consists of a moderator, a high-voltage input and a preamplifier. The counters operate under a gas pressure of 7bar (with an additional of 1%  $\text{CO}_2$ ). Each counter has a length of 50cm and a diameter of 3.2cm. The counters are housed in moderators which are made up of polyethylene material. The moderator consists of parallel planes that are placed 5cm apart. Neutrons entering the detector are slowed down for about 1 – 4 $\mu\text{s}$  when they reach the polyethylene material. Then after a few microseconds they diffuse into the moderator where they are either absorbed by the  $^3\text{He}$  counter or they escape detection. Fig 2.3 below shows a photo of the neutron counter and the moderator.

Detection of neutrons inside the counter occurs through the absorption of thermal neutrons according to the following reaction



As equation 2.1 shows one neutron can only be registered once, meaning that there is no “cross-talk” where one neutron can be detected more than once by the detectors. The helium counters do not give information about the energy of the neutrons, but that is not a concern as the objective of the setup is to measure the number of neutrons not their energies.

### 2.4.3 Electronics

The COMETA setup is a multi-detector system with PIN diodes used to provide both energy and time signals. For the time signal each PIN diode is used as a “stop” detector that provides the “stop” signal of fission fragments with the MCP providing the “start” signal. The two signals i.e. “start” and “stop” signals define the time-of-flight (TOF). The electronic components of the COMETA consist of three Constant Fraction Discriminators (CFD CF 8100), one for each mosaic from the two arms and the third one used for the “start” signal from the MCP detector. The time signal from the CFD of PIN diodes is delayed for 100ns and then sent to the Time to Digital Convertor (TDC Silena 4418). The

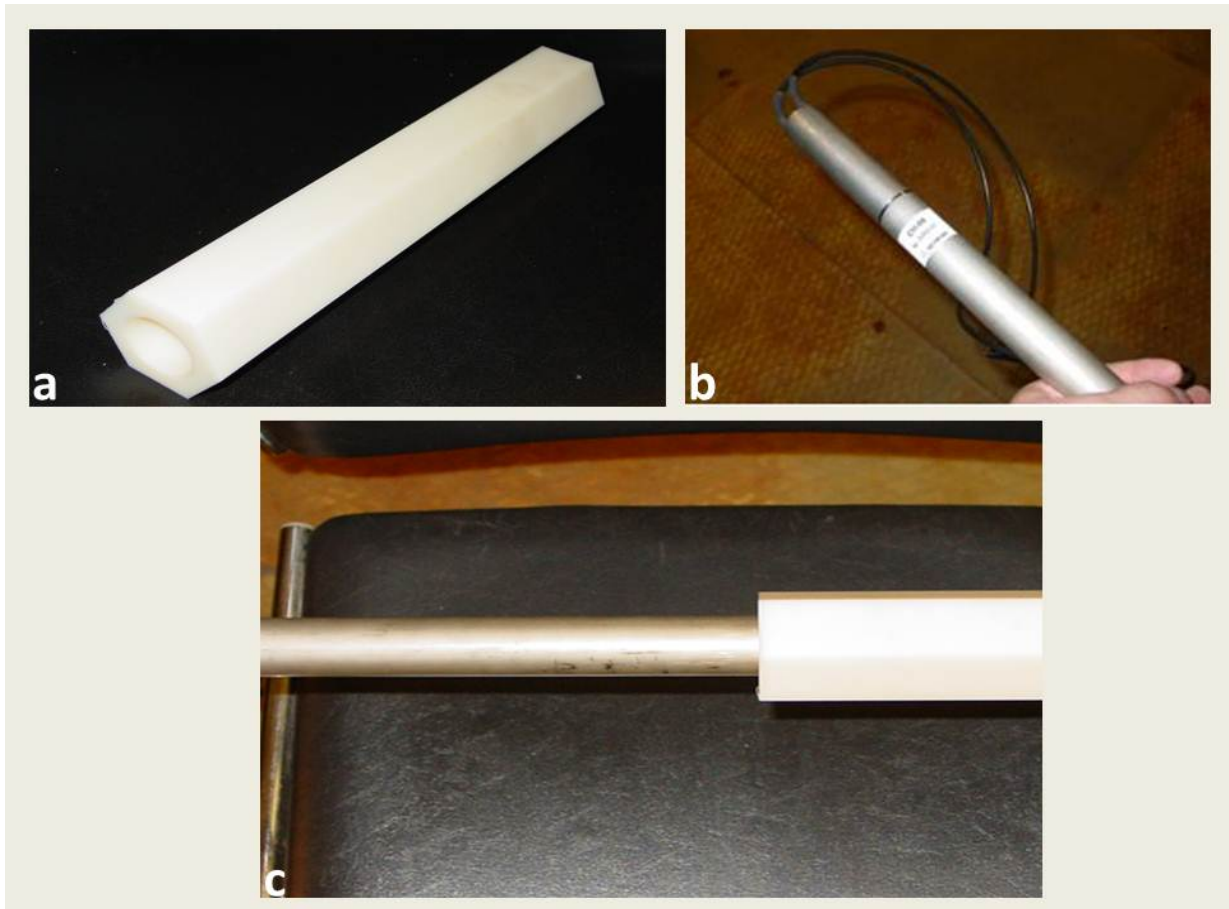


FIG. 2.3. Detector modules for Neutron counters. a) Shows the moderator, b) Neutron counter with high voltage input and preamplifier, c) the Neutron counter inside the moderator.

energy signal from the PIN diode on the other hand is delayed for  $200ns$  and then sent to the Charge to Digital Convertor (QDC Phillips Scientific 7166).

The time signal from the MCP “start” detector is delayed for  $30ns$  then sent to the coincident circuit before being taken to the start TDC. The time signal from the PIN diode is also sent to the coincident circuit which identifies fission event that take place in-coincidence. Three outputs for each event are produced from the coincidence circuit, one is the gate signal that is sent to the QDC, the second one is the start signal that is sent to the TDC, and the third one is the LAM (Look-At-Me) signal that is sent to the Analog Digital Convertor (ADC). The LAM signal is used by the data acquisition system to initiate data acquisition. The QDC, TDC, and ADC signals are sent to the CAMAC BUS which sends signals to the Crate Controller where the computer records the data from. The scheme for the electronics of the COMETA is shown in Fig 2.4.

## 2.5 Light Ions Spectrometer

### 2.5.1 Physical Motivation

Registering fission fragment energy with silicon based detectors comes with a challenge of pulse-height defect (PHD) which leads to the delay of energy signal. In general PHD is defined as the difference between the energy of a heavy ion and that of an alpha particle yielding the same pulse height. It is also known that the pulse height for a heavy ion is bigger than that of a light ion of the same energy. The other challenge is “plasma delay” which manifests itself with the reduction of the pulse rise time with decreasing  $Z$  proton number for lower intermediate mass fragments, for which the generated charge is completely absorbed by the detector.

Studies of PHD showed that its value consists of three components and each of them has a complicated dependence on the mass  $M$  and energy  $E$  of the registered fragment. It is also equally known that the energy  $E$  of the registered fragments is in turn dependent on the PHD value and the type of the detector used. The procedure that takes into account



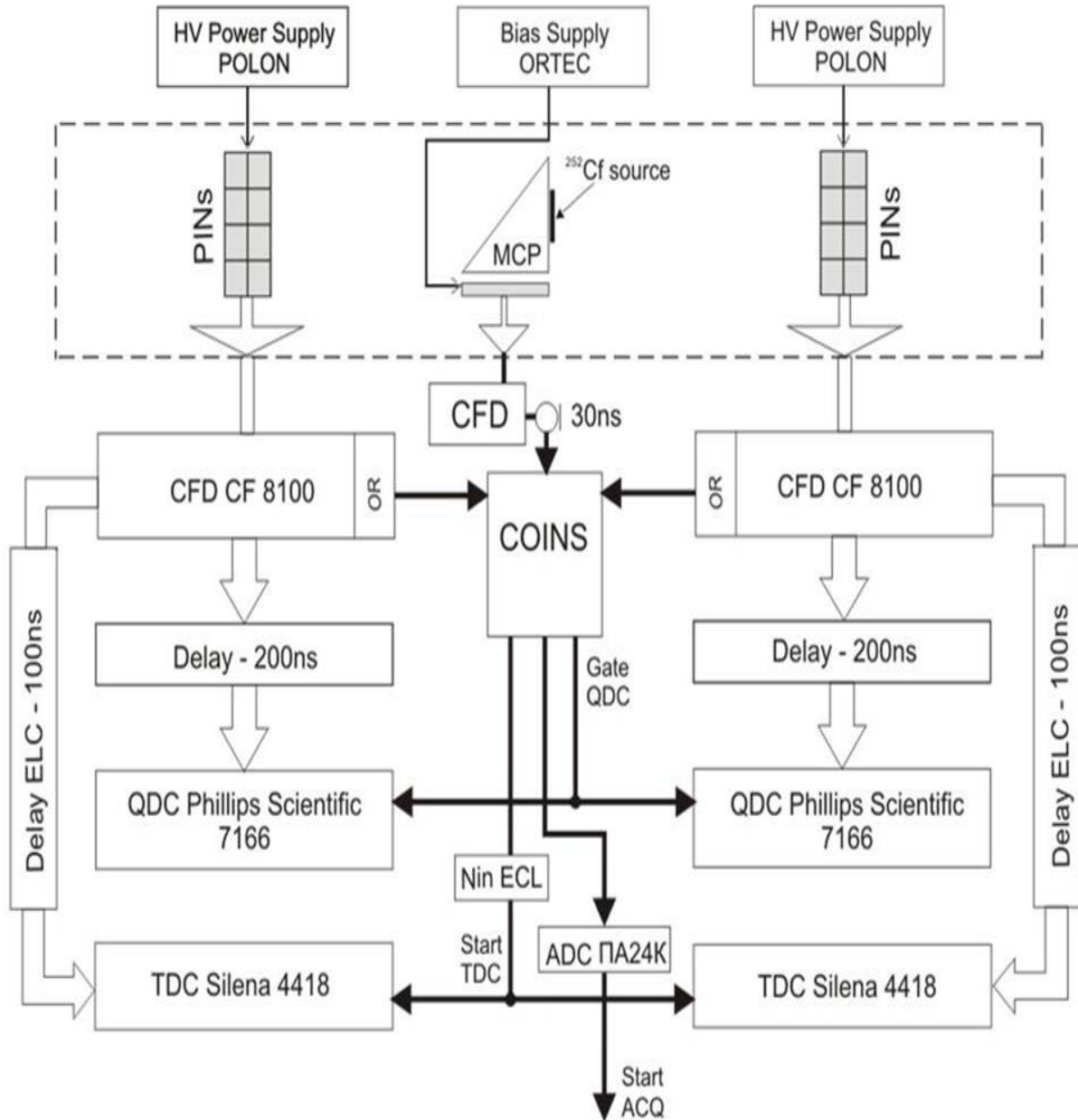


FIG. 2.4. Scheme for the electronics of the COMETA Spectrometer.

the PHD value for the registration of the fragments is discussed in chapter 3. In this section the focus is on a new setup designed to take into account the negative influence of the so called “plasma delay” when registering fragment time on the PIN diodes.

## 2.5.2 Description of the LIS Setup

The Light Ion Spectrometer (LIS) consists of three Micro-Channel Plate (MCP) timing detectors arranged as shown in Fig 2.5. The first MCP (referred to as “start” MCP) is

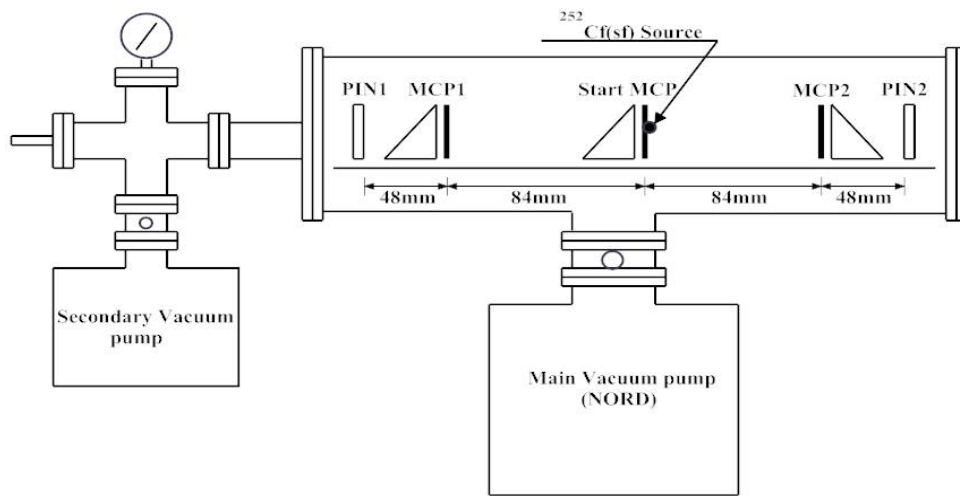


FIG. 2.5. Schematic view of LIS setup.

used to deliver a “start” signal and the other two MCPs (referred to as “stop” MCP1 from arm 1 and “stop” MCP2 from arm 2) are used to deliver a “stop” signal from both arms. The energy signal is measured from the two PIN diodes. PIN1 is used in the first arm and PIN2 is used in the second arm. The distance between the “start” MCP and both stop MCPs is  $84\text{mm}$  and the distance between each “stop” MCP and a PIN diode in the corresponding arm is  $48\text{mm}$  that makes the distance between the start MCP and each PIN to be  $132\text{mm}$  as shown in Fig 2.5. The size of each PIN is  $18\text{mm} \times 18\text{mm}$ . Note that for the LIS setup each arm consists of only one PIN diode detector.

LIS setup is installed in a specially designed two vacuum pump system, which consists of the main and secondary vacuum pump. The secondary vacuum pump is used to establish a vacuum of  $2 \times 10^{-2}\text{bar}$  after which the main vacuum is switched on to increase the

vacuum to  $2 \times 10^{-5} \text{bar}$ . The picture of the detector system for the LIS setup is shown in Fig 2.6 with the overall view of the setup shown in Fig 2.7.

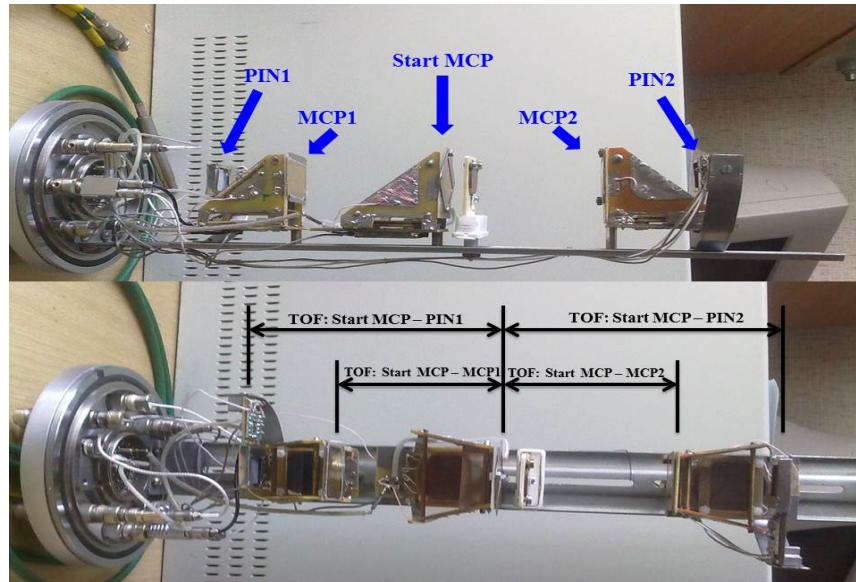


FIG. 2.6. Side and front view of the detector system of the LIS setup.

### 2.5.3 Electronics of the LIS Setup

The electronics scheme of the LIS setup is shown in Fig 2.8. As indicated in the scheme the energy or charge signal from each MCP detector is delayed for  $100 \text{ns}$  and then taken directly to the Charge to Digital Convertor (QDC Phillips Scientific 7166). The energy signal from each PIN diode is taken to the Constant Fraction Discriminator (CFD CF 8100) after which it is delayed for  $200 \text{ns}$  before being taken to the QDC. The following parameter labels are used for the energy signal scheme in the LIS setup:

Q1	Energy from PIN1
Q2	Energy from PIN2
Q9	Energy from “start” MCP
Q10	Energy from “stop” MCP1
Q11	Energy from “stop” MCP2

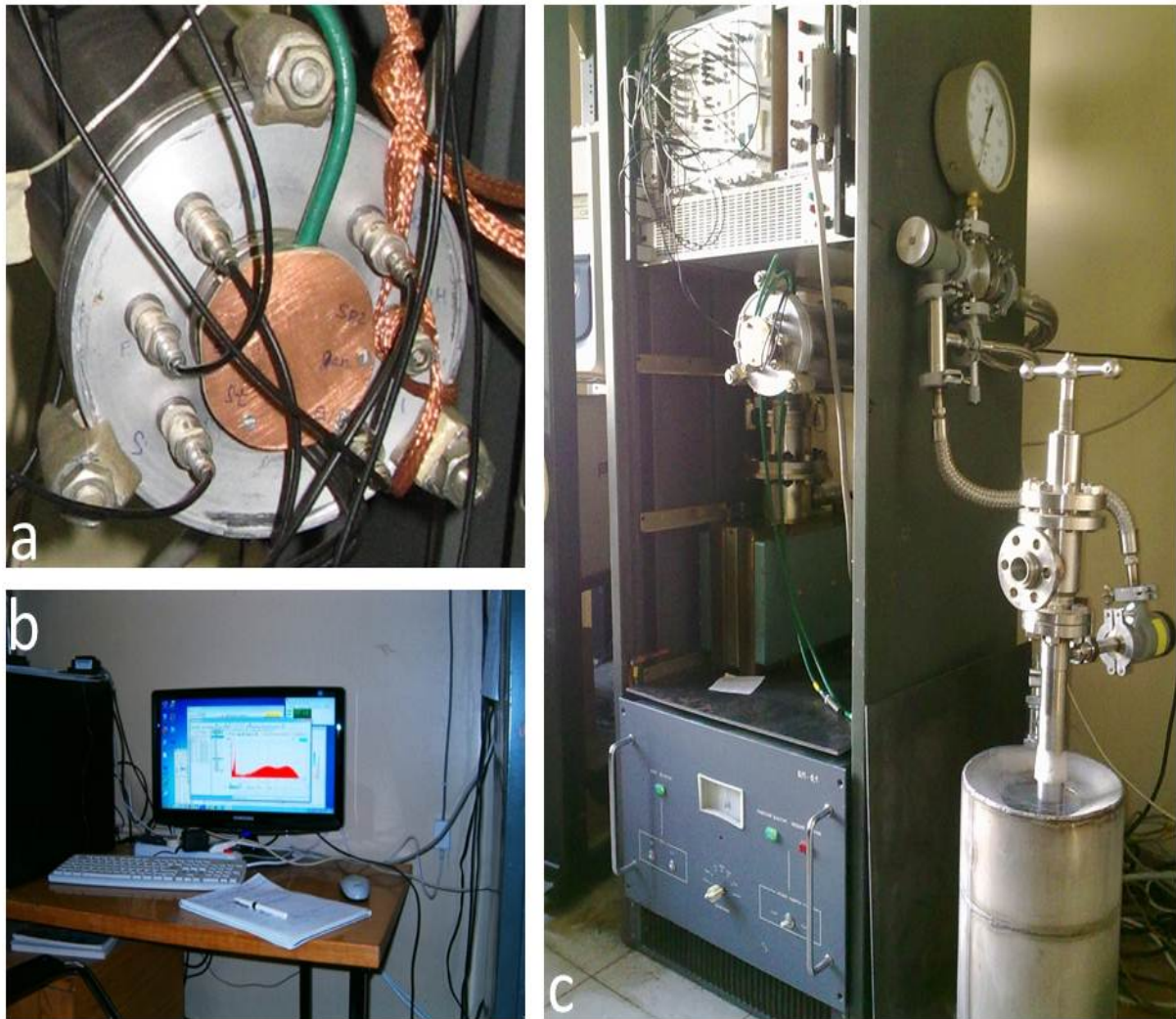


FIG. 2.7. Overview of the LIS setup, the connections of the detector system inside the vacuum chamber shown in (a), the data acquisition system shown in (b), and the overview of the LIS setup and some of the electronics shown in (c).

The time signal from all the MCP detectors is taken to the CFD and then delayed for  $100ns$  before being taken to the Time to Digital Convertor (TDC Silena 4418). The time signal from each PIN diode is taken to the CFD and delayed for  $100ns$  before being taken to the TDC. Label parameters for time signal are given below:

T1	Time signal from PIN1
T2	Time from PIN2
T6	Time signal from “start” MCP
T7	Time signal from “stop” MCP1
T5	Time signal from “stop” MCP2

The MCP start signal (T6) is split into two, with the first signal delayed for  $100ns$  before being sent to the TDC. The second signal is delayed for  $30ns$  before being sent to the coincidence circuit. The “OR” signals from the CFD of each PIN is sent to the coincident circuit to detect coincidence events. From the LAM signal onwards the electronic scheme for the LIS setup is similar to that of the COMETA setup.

## 2.6 Data Acquisition System

The data acquisition system for both the COMETA and LIS spectrometers is based on the FOBOS spectrometer data acquisition system [Ort98]. The entire system is composed of several computers with the x86 processor under the Win32 operating system (from Windows XP up to Windows 7). Use of these operating systems and the x86 processor provided the lab with the flexibility to scale up the computational power of the data acquisition system. The main feature of the data acquisition system is the possibility of the online accumulation of experimental data, pre-sorting and visualization of the data without reduction of the acquisition speed. This also provides the possibility to analyse data off-line. The major components of the data acquisition system are *WinELTEC*, *Mini-Client*, *Htask* and *Hoopsy32*.

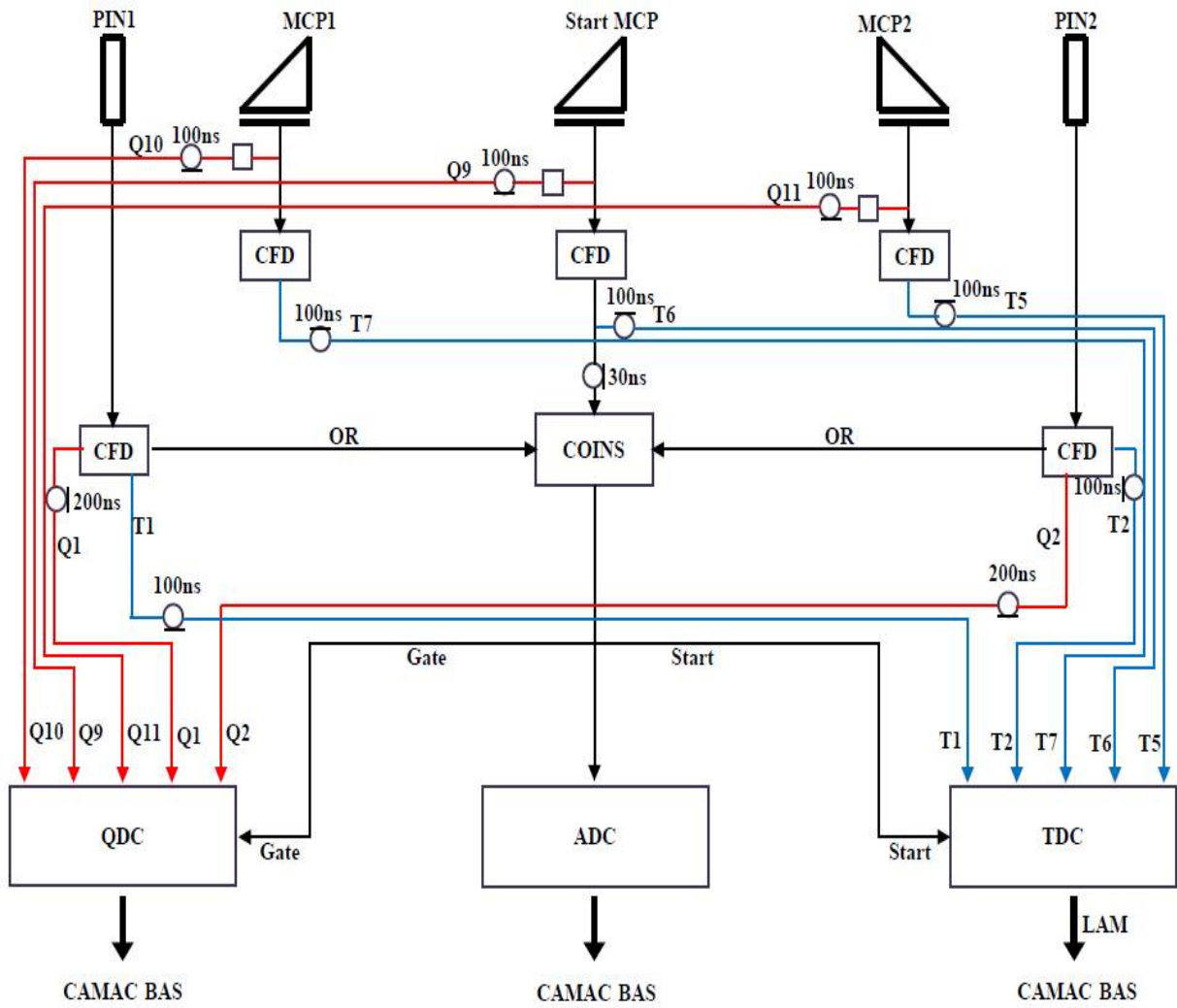


FIG. 2.8. Scheme for the electronics for LIS setup.

### 2.6.1 WinELTEC

WinELECT is a basic program-server whose main task is to control the modules of the CAMAC crate. The CAMAC crate itself is responsible for the collection of physical information from the experiment. The connections between the computer and the CAMAC crates are carried out by a specially designed PCI crate controller [Sem01] and the corresponding windows drivers. The WinELTEC program is also used in the initial set up of the CAMAC crate modules and controls the module parameters throughout the duration of the experiment. The operation of this program is triggered by a LAM signal from the crate controller.

### 2.6.2 Mini-Client

The Mini-Client is connected to the WinELECT and serves as a remote control for data acquisition. The main function of this program is to periodically acquire the number of slow changing system parameters and present them in a table format that can be viewed through a web-interface.

### 2.6.3 Htask

The Htask program prepares a configuration file that contains the description of all the experimental hardware to be used by WinELTEC. It can also be used as an emulator for the preliminary adjustment of the system.

### 2.6.4 Hoopsy32

This is the main program which connects directly to the WinELTEC according to the hardware description. Hoopsy32 collects and views all the experimental data and saves them into files. The features of this program allow the user to view the experimental spectra in one and two dimensions on-line. The user can also work with this program on the saved data files off-line.

### 2.6.5 HopRead32

The HoRead32 is a stand alone form of Hoopsy32. It only reads the data files created by Hoopsy32 and performs off-line processing and graphical representations of the experimental information stored on the files. The user can use this program to impose conditions on the one or two dimensional spectra using primary parameters already stored in the program or can use the user defined parameters.



# Chapter 3

## Data Analysis

### 3.1 Introduction

This chapter outlines all the processes and procedures involved in the analysis of data. The chapter is structured in the following way:

1. Determination of the detection efficiency of the neutron belt in the COMETA setup
2. Determination of the stability of the experimental data.

Determination of the detection efficiency of the “neutron belt” has two components. The first component is based on an earlier model used in the determination of the optimal configuration of the “neutron belt” detectors. This model is based on the Monte Carlo N-Particle (MCNP) code [Shu06] which simultaneously simulates the optimal configuration of the neutron detectors and the estimated detection efficiency. The second component involves the determination of detection efficiency using experimental data.

Determining the stability of the experimental data involves all the processes and procedures followed in tracking down any variations in the experimental data due to electronics and the rest of the equipment used to collect the data. This is then followed by the description of processes followed in the calculation of the masses of the fission fragments (FF). Reconstructing fission fragment masses is an involved and complicated task, as one needs to take into account effect of a so called pulse-height defect (PHD), as discussed in chapter 2.

This process is divided into two parts with the first focusing on the “first approximation” approach and the second on the “true energy calibration” approach.

In the “first approximation” the PHD value is approximated roughly and in the true energy calibration process the exact PHD value is calculated and used to reconstruct the mass of the FF. Lastly a process that takes into account a so called “plasma delay” in the registration of time-of-flight (TOF) using silicon detectors is discussed. Taking into account the plasma delay and the correct velocity measurement is the most important part of the data analysis process.

## 3.2 Detection Efficiency of the “Neutron Belt” of the COMETA Setup

As discussed in Chapter 2, the COMETA setup consists of 28  $^3\text{He}$  filled neutron counters that are positioned as a belt around a start detector of the COMETA setup. The neutron counters detect neutrons in coincidence with fission events. This means that when the fission event is registered by the mosaics, it triggers the neutron counters to open a gate for the detection of neutrons. However not only neutrons from the event that opened the gate are being detected, there are neutrons from previous fission events and experimental hall that are detected during the time interval when the gate is opened. Such neutrons are referred to as background neutrons. There is a complicated convolution between the neutrons from the fission event and background neutrons. The detailed process to analyze the detection of neutrons and calculate the detection efficiency is presented in the follow-up subsections.

### 3.2.1 Modeling of the “Neutron Belt”

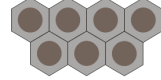
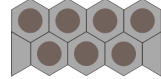
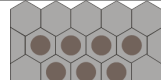
One of the key features of the COMETA setup is the “neutron belt”. The optimum configuration of the “neutron belt” was designed with the use of the Monte Carlo N-Particle (MCNP) simulation code. Different configurations were examined to arrange the neutron counters in the belt with the use MCNP code. Table 3.1 shows a comparison of the different configurations of the neutron counters. In order to obtain the best possible

configuration one needs to maximize the ratio between two probabilities. This ratio is given by

$$\frac{P_{iso}}{P_{mov}} \quad (3.1)$$

where  $P_{iso}$  is the the probability to detect neutrons from the isotropic source and  $P_{mov}$  is the probability to detect neutrons from the moving source. From the results of this modeling shown in Table 3.1 we simultaneously obtain the optimum configuration to use for the “neutron belt” and an estimation of the detection efficiency of each specific configuration which is given by the value of  $P_{mov}$ . For our purposes the optimum configuration is given in the first row of Table 3.1. The difference between the configurations shown in Table 3.1 is that extra moderators without neutron counters are added on the structures shown in raw two and three.

TABLE. 3.1. **Different configurations to arrange neutron counters in the belt.**

Configuration	$P_{iso}$	$P_{mov}$	$P_{iso}/P_{mov}$
	11.8%	5.23%	2.27
	16.17%	7.77%	2.08
	25%	13%	1.9

### 3.2.2 Calculating the Detection Efficiency of the “Neutron Belt” Using Experimental Data

It is well known that fission events are always accompanied by neutron emission. When a fission event is registered by the mosaics, it triggers the “neutron belt” to open a gate for the detection of neutrons emitted from that specific event. The challenge is that background neutrons from the experimental hall and previous fission events are also detected during this time interval. To solve this challenge, background neutrons are experimentally estimated by using a precise generator that emits up to four neutrons during specific intervals. This background is then subtracted from the neutron counts as explained below.

According to the probability theory, the probability for the neutron counters to detect  $i$  neutrons when  $n$  neutrons are emitted is given by the binomial probability law as follows:

$$P_{det-f}[k] = \sum_{k=i} P_{emit}[n] \varepsilon^i (1 - \varepsilon)^{n-i} C_i^n \quad (3.2)$$

where  $P_{det-f}[k]$  is the probability for neutron counter to detect  $k$  number of neutrons,  $P_{emit}[n]$  is the probability to emit  $n$  neutrons per fission of  $^{252}\text{Cf}$  nucleus,  $n$  is the number of neutrons emitted from fission events,  $i$  gives the number of neutrons detected by the neutron counters and  $\varepsilon$  is the detection efficiency to be calculated. The probability for the  $^{252}\text{Cf}$  source to emit neutrons is given in Table 3.2 and was obtained from literature [Tyu03].

TABLE. 3.2. **Probability of emission of  $n$  neutrons in  $^{252}\text{Cf}$  source.**

<b>n</b>	0	1	2	3	4	5	6	7	8	9
$P_{emit}[n]$	0.0025	0.0282	0.1199	0.2681	0.3056	0.1951	0.0674	0.0084	0.0045	0.0004

Equation 3.2 allows us to calculate the probability of detecting neutrons from fission events without background. In order to develop a precise procedure for the calculation of the detection efficiency of the neutron counters, background neutrons should be taken into account. To this end the neutron generator, as was mentioned above, was used to estimate background neutrons. Thus, if  $P_{gen}[j]$  is the probability of neutron counters to detect neutrons emitted by the generator, then the experimental expected number of neutrons to be detected denoted by  $P_{exp}[i]$  is given by:

$$P_{exp}[i] = \sum_i P_{det-f}[k] \times P_{gen}[j] \quad (3.3)$$

where  $j$  is the number of neutrons emitted by the generator. The distribution that we obtain from equation 3.3 should correspond to the experimental data since it includes the background neutrons. From equation 3.3 it is clear that the experimental distribution for the number of detected neutrons is a convolution of neutrons from fission events and background neutrons.

In order to calculate the detection efficiency denoted by  $\varepsilon$  in equation 3.2, a fitting process was applied where different distributions were calculated using equation 3.3. These distributions were then compared with the experimental data. The comparison process

was performed using a specially designed C++ program. The different distributions were calculated using different detection efficiencies, i.e. 3.75%, 4.00%, 4.25%, 4.5%, 4.75%, and 5.00%. The fitting process was then performed with the experimental data to determine the correct detection efficiency for the neutron belt. The distribution that gave a best fit was obtained with the detection efficiency of 4.25%. This best fit for the COMETA setup neutron belt detection efficiency is shown in Fig 3.1. The complete algorithm of the entire

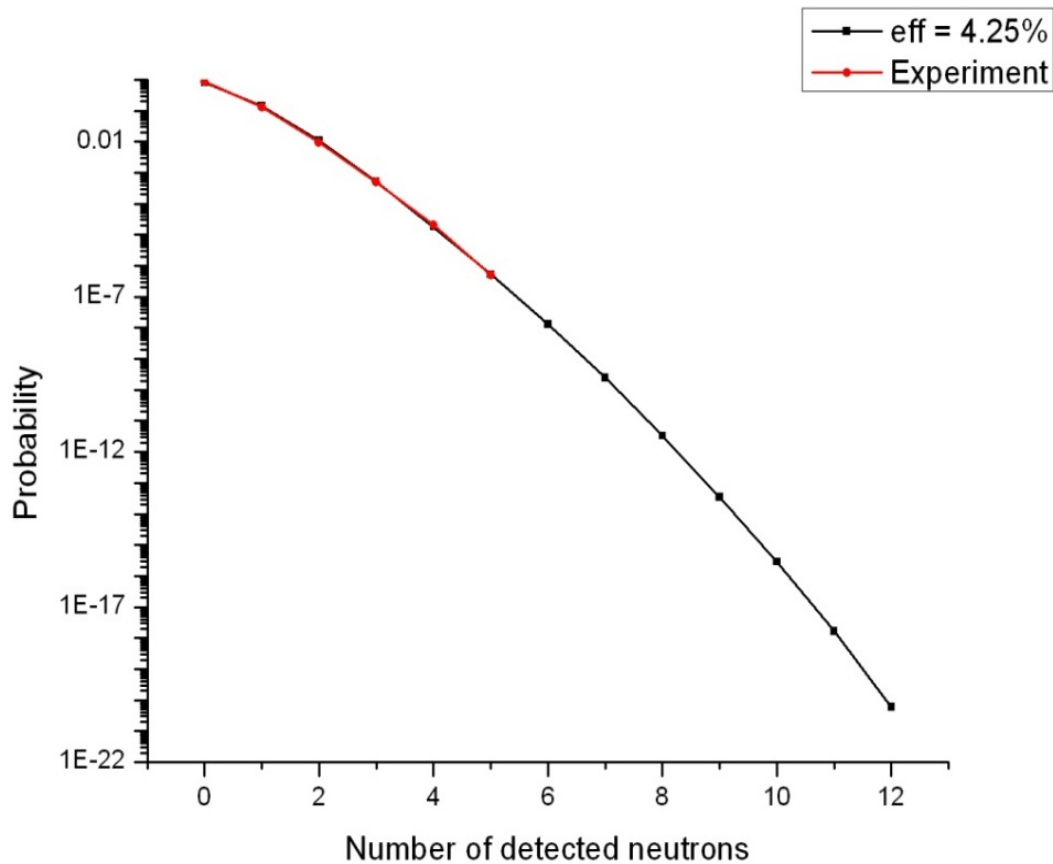


FIG. 3.1. Comparing the experimental data with the calculated distribution at  $\varepsilon = 4.25\%$ .

process of calculating the detection efficiency is shown in Fig 3.2. As it can be seen from the algorithm, the probability for the fission source to emit neutrons is used to calculate the probability for the neutron counters to detect neutrons and this probability is free from background neutrons. The neutron generator is used to simulate background neutrons and from the spectrum obtained the probability for background neutrons is then calculated.

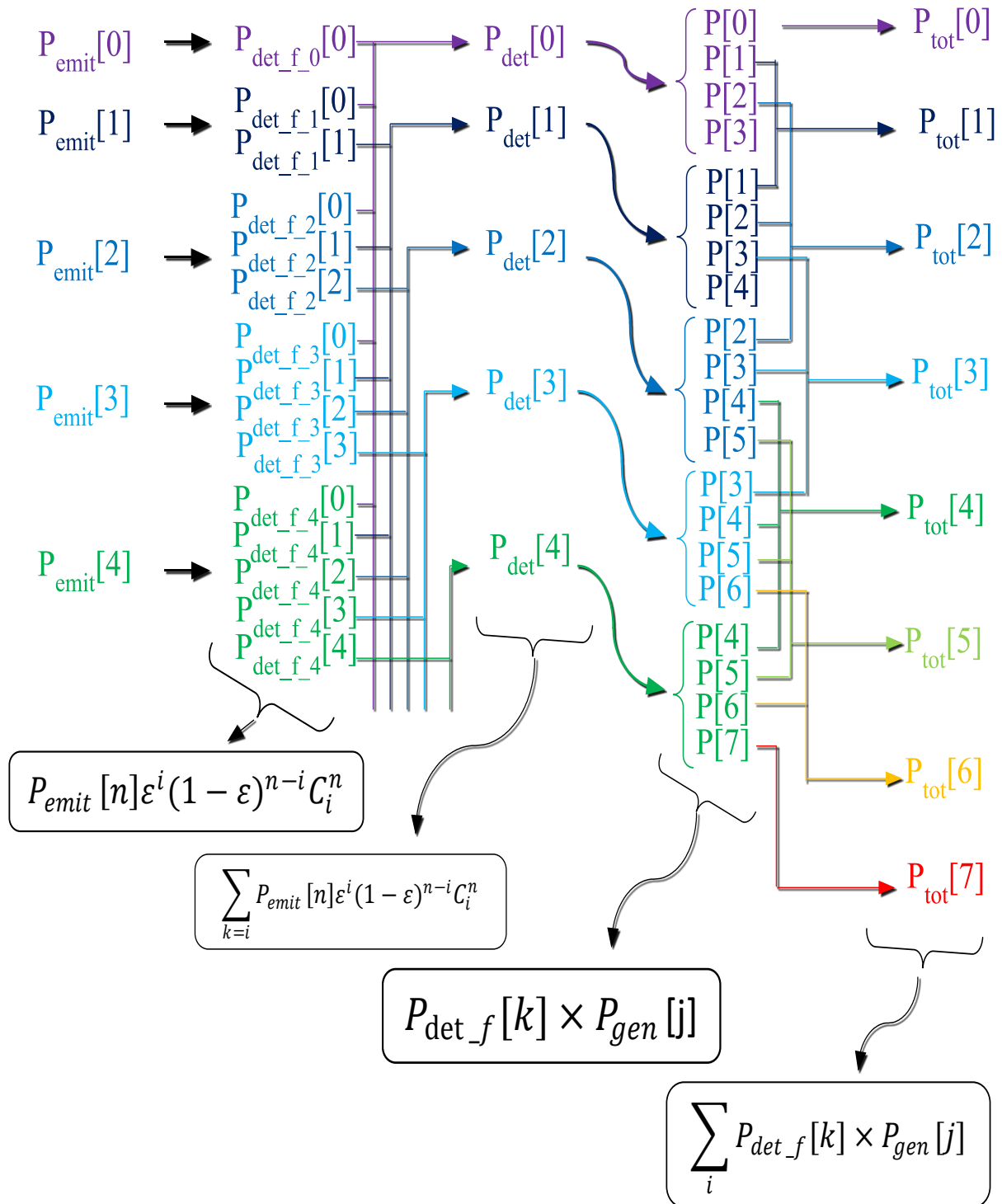


FIG. 3.2. Algorithm for the entire process to obtain the calculated distributions.

Thereafter, the convolution of the probability to detect neutrons from the fission source and the probability to detect the background neutrons is calculated using equation 3.3. The distribution from the convolution is then fitted with the experimental data to obtain the correct detection efficiency. The detection efficiency is then used to calculate the neutron spectrum without background neutrons. This spectrum is shown in Fig 3.3. The comparison between the distribution with background neutrons and without background neutrons is shown in Fig 3.4. It is clear from Fig 3.4 that background neutrons have more influence at low probabilities.

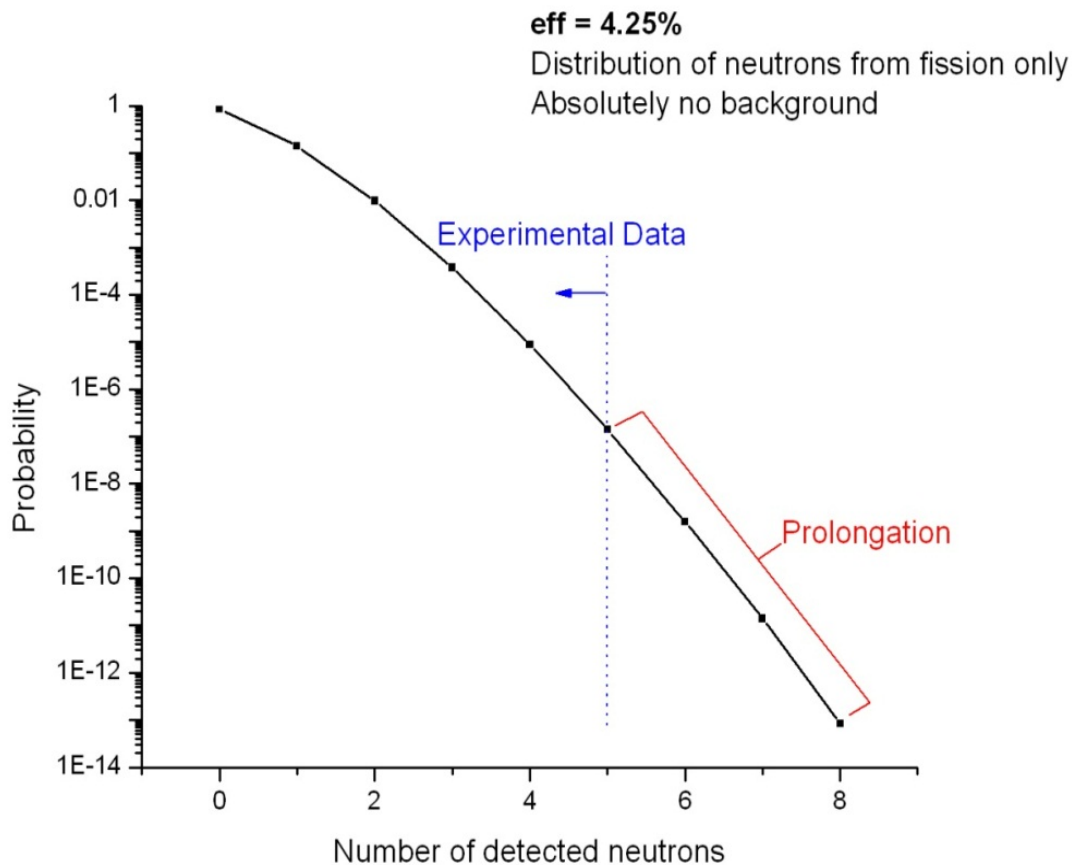


FIG. 3.3. Number of detected neutrons from fission events only with no background.

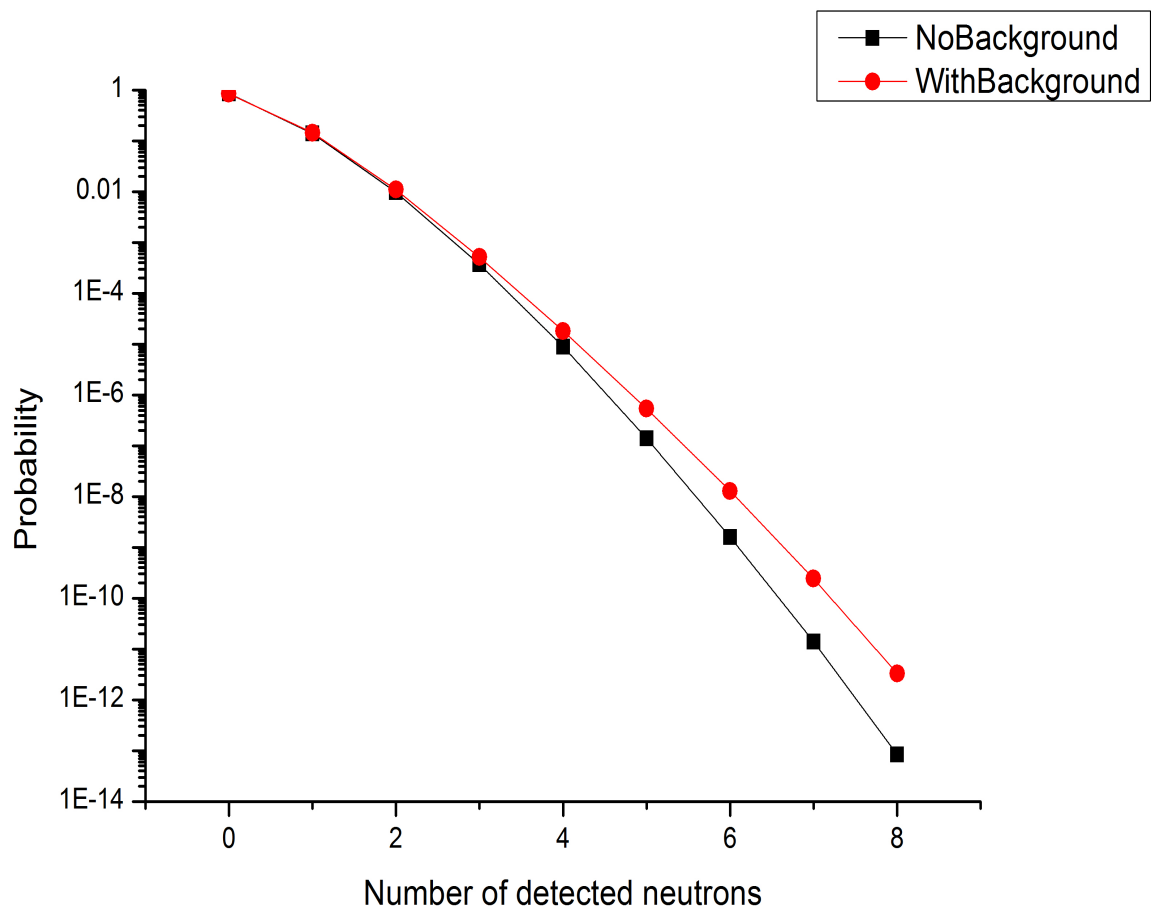


FIG. 3.4. Comparison between the distribution with background neutrons and without background neutrons.



### 3.3 Data Stability

Data stability tests are performed to ensure that data is free from variations due to electronics used in the experiment. When testing the stability of the data, the possibility of having any variations in all the energy ( $E$ ) and time ( $T$ ) channels is investigated. The data acquisition system used for the experiment can automatically perform some preliminary cross-checks of the data stability parameters, but a detailed analysis is always required.

A stability test is performed by calculating the *mean* value and the *dispersion* of the data in a spectrum. In statistics, mean and dispersion are one of the parameters obtained from the *sampling* process. Sampling is an experimental method used to obtain information about parameters of an unknown distribution [Leo94]. A brief explanation of this method is given below.

Consider a sample  $x_1, x_2, \dots, x_N$  of size  $N$ , the sample mean  $\bar{x}$  is defined as

$$\bar{x} = \frac{1}{N} \sum_{i=1}^N x_i \quad (3.4)$$

And the sample variance is defined as

$$\sigma^2 = \frac{1}{N} \sum_{i=1}^N (x_i - \bar{x})^2 \quad (3.5)$$

The square root of the variance is called standard deviation and denoted by  $\sigma$ . The variance is therefore given by the average squared deviation of  $x$  from the mean. The standard deviation thus measures the dispersion of the distribution and gives an idea of how much the random variable  $x$  fluctuates about its mean [Leo94].

A special program for analyzing data stability including the formalism given above was written using FOTRAN 99 code. For data stability each PIN diode detector is analyzed individually and the energy and time channels are read separately from the data file. For each channel, the events are divided into groups of 1000 events (due to the large number of events obtained from the experiment) and the mean for each group is calculated. The plot for the mean versus the group of events for the time channel from PIN-21 (the first PIN diode from the second arm) of the COMETA setup is shown in Fig 3.5. Note that

each point in Fig 3.5 represents a mean of 1000 events.

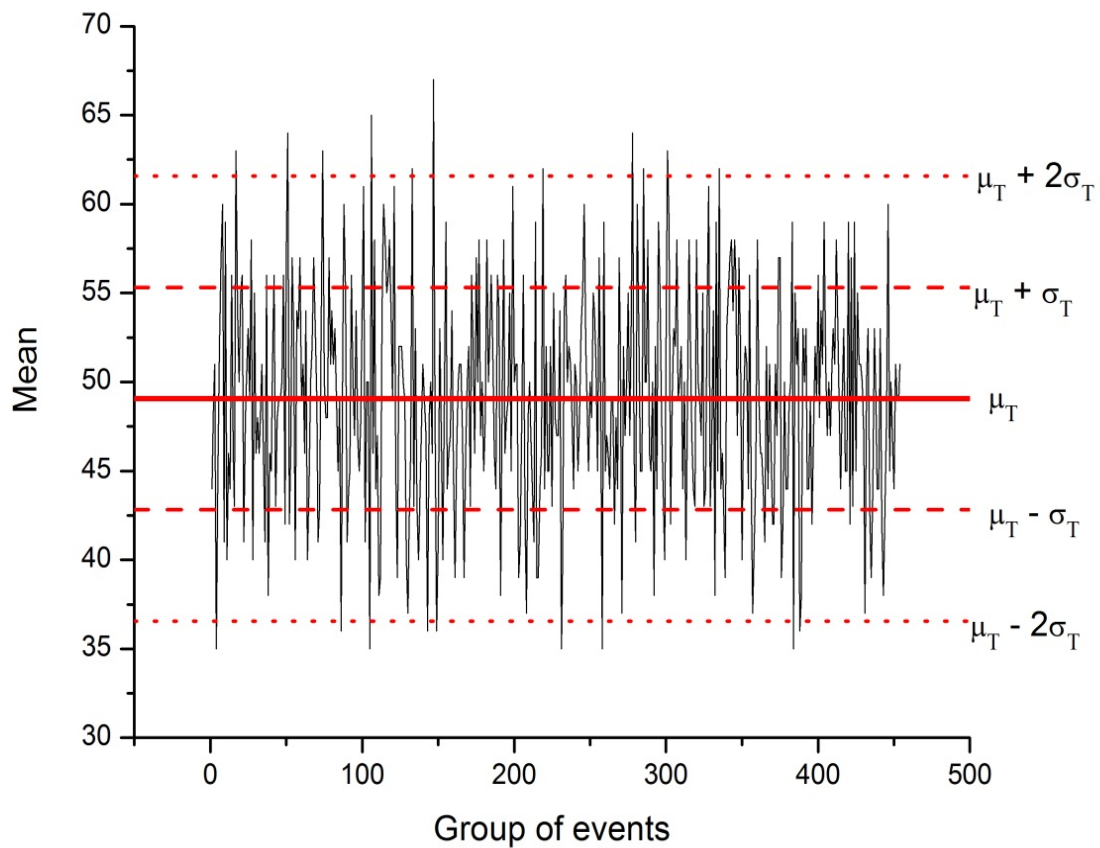


FIG. 3.5. Mean value  $\mu_T$  of time channel from PIN-21 versus the group of events.

### 3.3.1 Results of Data Stability Test

The aim of performing data stability is to test for instrumental errors which are best described by a Gaussian distribution. Therefore a Gaussian distribution is assumed in the data in order to apply its techniques for the analysis. The mean  $\mu_T$  for the time channel distribution of PIN-21 has been calculated and is shown by the horizontal solid line in Fig 3.5.

According to the Gaussian distribution, approximately 68% of data points should lie in the interval  $\tilde{\mu}_T \pm \tilde{\sigma}_T$  and 95.5% of data points should lie in the interval  $\tilde{\mu}_T \pm 2\tilde{\sigma}_T$  to obtain a stable data. As shown in Fig 3.5 only less than 5% of the data points lie outside the interval  $\tilde{\mu}_T \pm 2\tilde{\sigma}_T$  meaning that the time channel from PIN-21 is stable. The same procedure is followed for all the energy and time channels of each PIN diode used in the experiment.

In instances where data input channel is unstable, a reason for the instability is investigated. There are couples of factors that can affect the stability of the data, with the two obvious ones being, old or faulty electric cables and variations in room temperature. Temperature however has a greatest influence on the stability of the data. The obvious precaution is to ensure stability in the data is to make sure a stable room temperature is maintained and electrical cables are maintained or replaced timeously.

### 3.4 Reconstruction of the Fission Fragment Masses

Reconstruction of the fission fragment masses is dependent on the proper registration of fission fragment energies. To perform the correct mass calculation for the fission fragments a special calibration process has been developed at Flerov Laboratory. It was mentioned in chapter 2 that registering the energy of fission fragments (FF) with the use of silicon detectors presents its own set of challenges. One of these challenges is factoring in the effect of pulse-height defect (PHD) as was explained in chapter 2. Studies of PHD show that its value consists of three components (see equation 3.6) with each having a complicated dependence on the mass  $M$  and energy  $E$  of the registered fragment. The value of the PHD ( $R(M, E)$ ) can be obtained from the following equation:

$$R(M, E) = R_w(M, E) + R_n(M, E) + R_{rec}(M, E) \quad (3.6)$$

Where  $R_w(M, E)$  is associated with the loss of energy in the entrance window of the detector,  $R_n(M, E)$  is associated with the energy lost during the collision of heavy ions with the atoms of crystal lattice in the detector and  $R_{rec}(M, E)$  is associated with the recombination of electron-hole pairs in the plasma produced along an ion track. Determining the value of  $R(M, E)$  is challenging as it depends on many factors that relate to both the detected particle and the properties of the detector. The best methods to calculate this value are

based on the application of empirical formulas. For the purpose of our data analysis a new empirical formula for PHD description for PIN diodes based on the derivation of *Mulgin et al* [Mul97] has been used and is explained below.

The first step of the calibration process comprises the selection of raw data and performs a direct transformation of channel energies to Mega-electron Volts ( $MeV$ ). In this step the PHD is approximated roughly and the step itself is usually referred to as the “first approximation”. In the second step a so called “true calibration” process is performed where the exact value of the PHD is calculated and used to reconstruct the masses of the fission fragments. A detailed explanation of these steps is given below.

### 3.4.1 The “First Approximation” Approach

The “first approximation” is based on the simple transformation of energy and time in channels into  $MeV$  and nanoseconds  $ns$  respectively. The mass of the fission fragments in atomic mass units ( $amu$ ) is calculated using these values. This approach does not take into account the energy lost in the entrance window of the “start” detector and the source backing. The PHD is roughly estimated during this phase and “plasma delay” in the time signal is also not taken into account. During this phase raw data is read and transformed into the necessary required units. Channel energies are converted into  $MeV$ 's according to the following equation:

$$E_i[MeV] = C \cdot \exp\left(-\frac{E_i[ch]}{D}\right) + E_0 \quad (3.7)$$

The values of  $C, D, E_0$  are determined by using the known positions for the energy peak of light and heavy fragment and the natural alpha peak of  $^{252}Cf$  with  $E_\alpha = 6.118MeV$  as shown in Fig 3.6. The subscript  $i$  in equation 3.7 shows that each event is processed individually.

Time in channels  $T[ch]$  is converted into nanoseconds  $T[ns]$  according to the following equation:

$$T_i[ns] = A \cdot T_i[ch] + B \quad (3.8)$$

The values  $A, B$  are determined by using the known velocities  $V_{L,H}^{ref}$  of light (L) and heavy (H) fragment from literature [Sch83]. The experimental expected time-of-flight in nanosec-

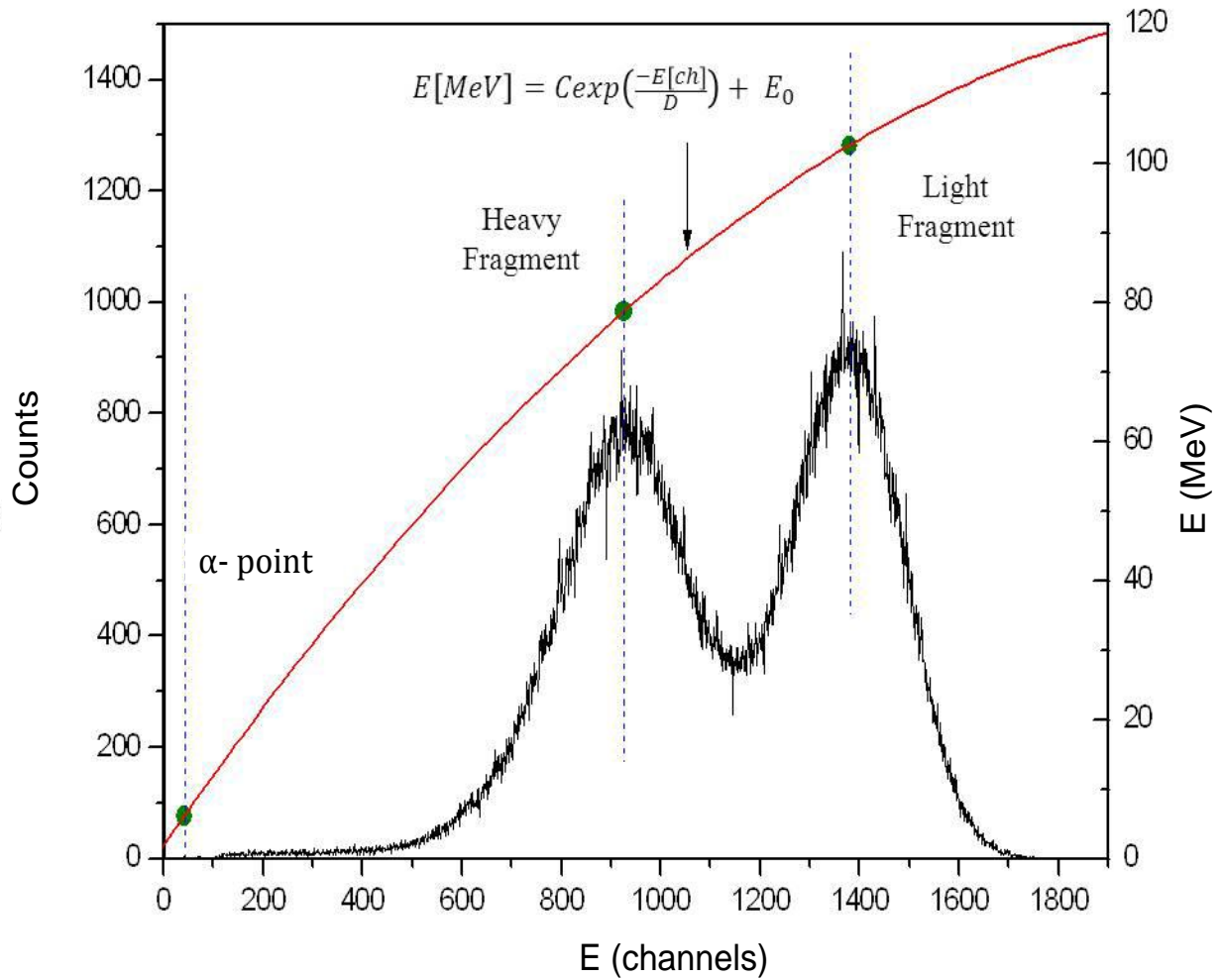


FIG. 3.6. Illustration of first approximation energy calibration.

onds of the light and heavy fragment is calculated as follows:

$$T_{L,H} = \frac{L_{TOF}}{V_{L,H}^{ref}} \quad (3.9)$$

where  $T_{L,H}$  is the time-of-flight of the light and heavy fragment and  $L_{TOF}$  is the flight path of the fission fragments. Knowing the values of  $T_{L,H}$  from equation 3.9 one can calculate the value of  $A$  as follows:

$$A = \frac{T_H[ns] - T_L[ns]}{T_H[ch] - T_L[ch]} \quad (3.10)$$

The value of  $B$  is calculated as follows:

$$B_{H,L} = T_{H,L}[ns] - A \cdot T_{H,L}[ch] \quad (3.11)$$

There is however a significantly small difference in the values on  $B_{H,L}$  obtained for the heavy fragment and that obtained for the light fragment. The average between the two  $B$  values is calculated as follows:

$$B = \frac{B_H + B_L}{2} \quad (3.12)$$

Once the values of  $A$  and  $B$  have been calculated, equation 3.8 is then used to convert channel time into nanoseconds. This time is then used to calculate the velocity of the fragments in centimeters per nanoseconds as shown below

$$V_i[cm/ns] = \frac{L_{TOF}}{T_i[ns]} \quad (3.13)$$

Using equation 3.7 and 3.13 one can calculate the mass of the FF as follows:

$$M_i[amu] = \frac{1.9297E_i[MeV]}{(V_i[cm/ns])^2} \quad (3.14)$$

After processing all the individual events, a mass spectrum is obtained. The ‘‘First Approximation’’ approach is illustrated in Fig 3.7.

### 3.4.2 True Energy Calibration and Reconstruction of FF Masses

The reconstruction of the FF masses follows a specially designed process which constitutes calculation of the true energy of the fragments. The main idea behind this procedure is to calculate the FF mass spectrum  $Y_{ex}(M_{TE})$  with the relevant parameter values and compare it with a known one from the literature [Wah88]. This procedure is applied to every single

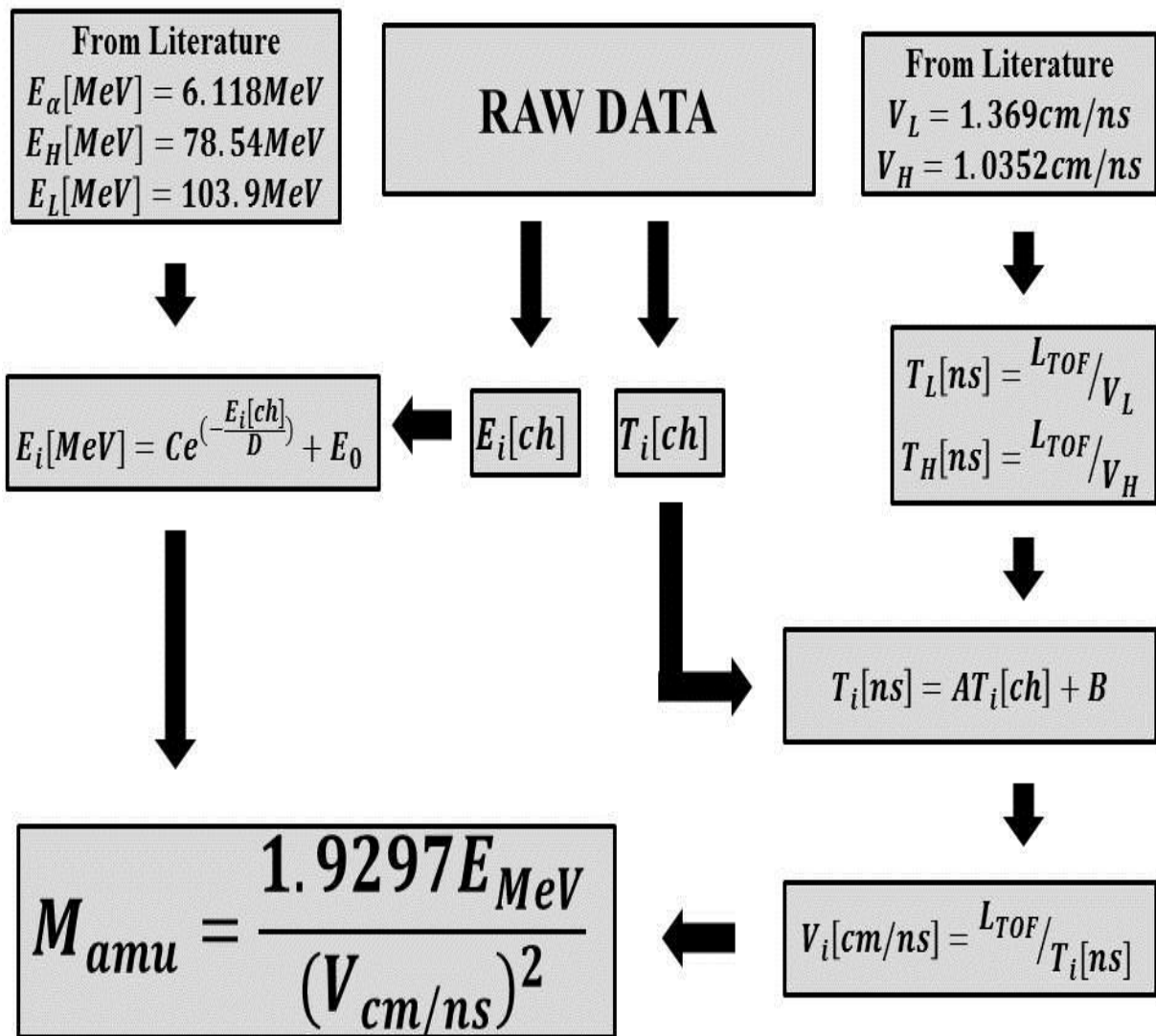


FIG. 3.7. The "first approximation" approach in the FF masses reconstruction.

detector. The energy  $E$  in  $MeV$ , of the registered fission fragment is defined as the sum of the detected energy  $E_{det}$  and the pulse-height defect denoted by  $R(M, E)$ :

$$E = E_{det} + R(M, E) \quad (3.15)$$

where the detected energy of fission fragments is given by:

$$E_{det} = E[ch] \cdot E_k + E_0 \quad (3.16)$$

where  $E_k$  and  $E_0$  are calibration parameters. These parameters are calculated experimentally by using a high precision pulse generator (ORTEC 448 Research Calibrator) and natural alphas for  $^{252}Cf$  source. The expression for the pulse-height defect in equation 3.15 was proposed by *Mulgin et al* [Mul97] and is given as follows:

$$R(M, E) = \frac{\lambda \cdot E}{1 + \phi \cdot \frac{E}{M^2}} + \alpha \cdot ME + \beta \cdot E \quad (3.17)$$

where  $\lambda, \phi, \alpha, \beta$  are parameters for the “true calibration”. In addition we know that:

$$E = \frac{M \cdot V^2}{1.9297} \quad (3.18)$$

where  $E$  is the energy of the FF in  $MeV$ ,  $M$  is the mass of the FF in  $amu$  and  $V$  is the velocity of the FF in  $cm/ns$ . The velocity, for this purpose is calculated using the parameters obtained from time calibration. From the above equations, we can calculate the mass of the fission fragment provided the parameters  $\lambda, \phi, \alpha, \beta$  are known. It is worth mentioning that the numerical values for the parameters  $\lambda, \phi, \alpha, \beta$  proposed in [Mul97] make it impossible to reconstruct the mass  $M_{TE}$  of the FF due to the different type and size of the PIN diodes used in the experiment.

In order to find the correct values of the parameters  $\lambda, \phi, \alpha, \beta$  a special iteration procedure has been designed. This procedure involves obtaining an analytical solution of the following equation:

$$G((\lambda, \phi, \alpha, \beta), M) = 0 \quad (3.19)$$

where  $G$  is an analytical function that depends on the parameters  $\lambda, \phi, \alpha, \beta$  and the mass  $M$ . To obtain the solution of equation 3.19 above, equations 3.15, 3.17, and 3.18 are



combined to give the following equation:

$$\frac{MV^2}{k} = E_{det} + \frac{\lambda \cdot \frac{MV^2}{k}}{a + \phi \cdot \frac{MV^2}{Mk}} + \alpha \cdot \frac{M^2V^2}{k} + \beta \cdot \frac{MV^2}{k} \quad (3.20)$$

where  $k = 1.9297$  is the constant value. The above equation can be written as follows:

$$M^3 + aM^2 + bM + c = 0 \quad (3.21)$$

with

$$a = \frac{\phi V^2}{k} + \frac{\beta + \lambda - 1}{\alpha} \quad (3.22)$$

$$b = \frac{kE_{det}}{\alpha V^2} + \frac{\phi V^2}{\alpha k}(\beta - 1) \quad (3.23)$$

$$c = \frac{\phi E_{det}}{\alpha} \quad (3.24)$$

It is clear that equation 3.21 is a third order equation; therefore its solution consists of three roots. There are few possibilities for obtaining the roots of this equation depending on the nature of the roots which is described by the discriminant ( $\Delta$ ) of equation 3.21. In this iterative process only positive real roots taken into consideration with negative and complex roots neglected. The selected roots are then compared to the value of the mass obtained from the “first approximation”. A special program for this purpose was designed using FOTRAN-99 code.

Using the above procedure events from the raw data are processed individually based on the current values of  $\lambda, \phi, \alpha, \beta$  and mass of the fission fragments is calculated. This mass is calculated under the condition that  $M_{TE} \in [1amu, 252amu]$ . This procedure is accomplished with the use of the MINUIT package [Jam94] to minimize the following criterion function by changing the parameters  $\lambda, \phi, \alpha, \beta$ :

$$F = [(\langle ML_T \rangle - \langle ML \rangle)^2 + (\langle MH_T \rangle - \langle MH \rangle)^2] + \mu \sum_{M_{TE}} \frac{(Y(M_{TE}) - Y_T(M_{TE}))^2}{Y(M_{TE})} \quad (3.25)$$

where  $\mu$  is a free parameter that is chosen by the user and used as an input parameter to the MINUIT minimization procedure. This parameter plays a role of specific relative weight of the second term in the criterion function  $F$ . The values  $\langle ML \rangle$  and  $\langle MH \rangle$  are

average masses of light and heavy fragments calculated from the experimental mass spectrum  $Y(M_{TE})$ .

In the above equation (equation 3.25) the known values from literature are denoted by “ $T$ ”. It is worth noting that the first square bracket term in equation 3.25 is sensitive to the difference between the centers of the mass peaks for the fission fragments. The second term is responsible for the agreement in shapes between the experimental mass spectrum and the mass spectrum from literature  $Y_T(M_{TE})$ . The quantitative criterion of the correct fit of the second term in equation 3.25 is based on the Chi-Square distribution. The algorithm for the “true calibration” approach is shown in Fig 3.8.

## 3.5 “Plasma Delay” and Correctness of the Velocity Measurement

As was explained in chapter 2 the CCT fragments differ radically in their masses. This therefore means that measuring the correct energy and time-of-flight of heavy ions in this wide range of energies and masses using PIN diodes as “stop” detectors presents us with two challenges. The first one being the PHD as was explained above and the second is the “plasma delay”. Below we discuss challenges related to “plasma delay”.

### 3.5.1 “Plasma Delay”

It is known very well that the pulse formation in the silicon detectors is slowed down for energetic heavy ions when compared with protons or alpha particles. Beside the increase of the pulse rise time referred to as “plasma time” there is also an issue of “plasma delay” as reported in [Alb69], [Mos71]. While there is no real delay in the beginning of pulse formation, fission fragment pulses are registered a few seconds later than alpha and proton pulses. Despite the use of the fraction discriminator which should have taken care of “plasma time” and amplitude fluctuations [Han78]. This extra delay referred to as “plasma delay” seems to be caused by a change of pulse shape as shown in Fig 3.9. The distance ( $d$ ) in the figure between the intersections of the extrapolated linear part of the pulse with the base line is approximately equal to the “plasma delay” difference measured with a

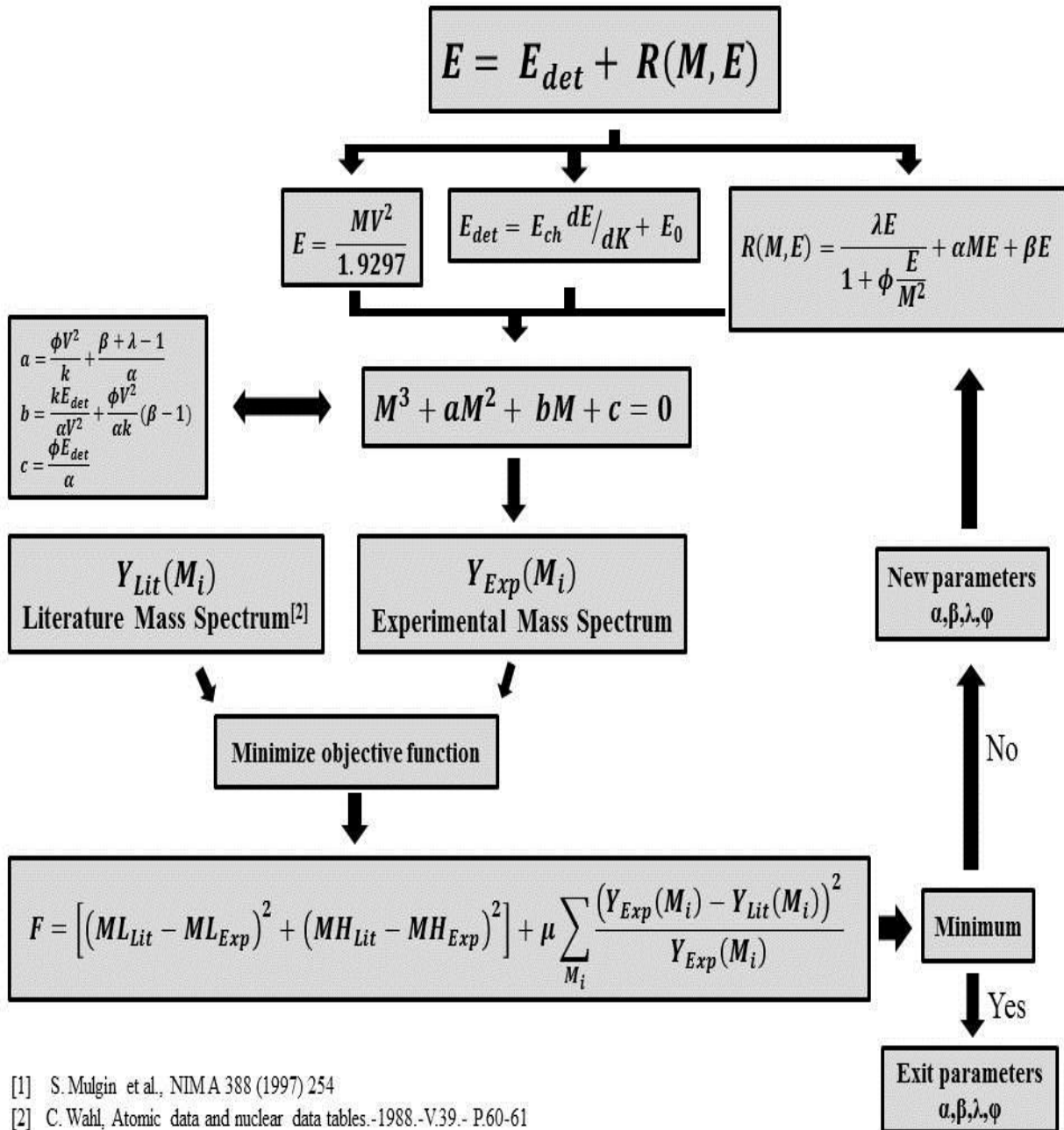


FIG. 3.8. The “true energy calibration” approach and reconstruction of FF masses.

CFD [Han78], [Nei83].

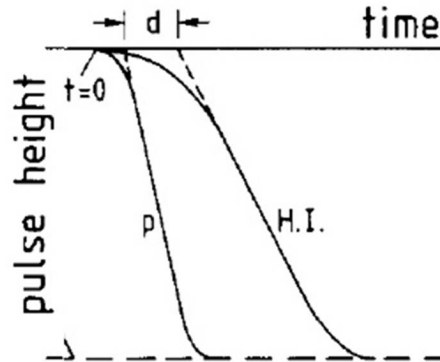


FIG. 3.9. Illustration of “plasma delay” for heavy ions (*HI*) compared to protons (*p*) as defined in [Han78] and [Nei83].

### 3.5.2 “Plasma Delay” Correction

The commonly used method to correct the effect of “plasma delay” is to measure the TOF spectra at two different distances and extrapolate the peak position to zero. This method was earlier used by *Kim Y.S. et al* in their study of the *Double arm fission fragment spectrometer* [Kim93]. This method was however not too reliable and *Kim Y.S. et al* had to use an alpha emitter as a calibration source and the so called *Neidel* and *Henschel* formula [Nei80] to calculate “plasma delay”.

In our study the influence of “plasma delay” was solved by designing a special spectrometer called *Light Ion Spectrometer (LIS)*. LIS measures the TOF using two Micro-Channel Plate (MCP) timing detectors placed in the same line producing a flight path of the fission fragment between each other. This idea uses one MCP as a “start” detector and the next one as a “stop” detector, thus measuring the timing signal from the MCP detectors (see also Fig 2.5 - 2.8). This is to ensure that the timing signal is free from plasma delay influence.

# Chapter 4

## Results and Conclusion

### 4.1 Introduction

After the design and construction of the Light Ions Spectrometer (LIS) was completed a number of tests were performed to check the reliability and operation of the system. A first experiment with a  $^{252}\text{Cf}$  source was performed using the calibration procedure described in the previous chapter. Data obtained from this first experimental run was processed and compared with known results from literature. The focus of this chapter is the analysis of the data from the LIS experiment and the presentation of the results.

### 4.2 The First Experimental Results from LIS setup

The mass spectrum obtained from the LIS setup is presented in Fig 4.1 below. The figure shows mass distributions from PIN1 (Mte 1 PIN) and PIN2 (Mte 2 PIN) obtained using the true calibration procedure explained in chapter 3. The distributions are compared to the known mass distribution of fission fragments of  $^{252}\text{Cf}$  from literature [Wah88].

It can be seen from the figure that the data from our experiment agree well with spectrum from literature. Specific parameters obtained from the experiment which can be deduced from the spectrum in Fig 4.1 are shown in Table 4.1. The mean of the mass of the light fragment  $\langle M_L \rangle$  in atomic mass units and the mean of the mass of the heavy fragment

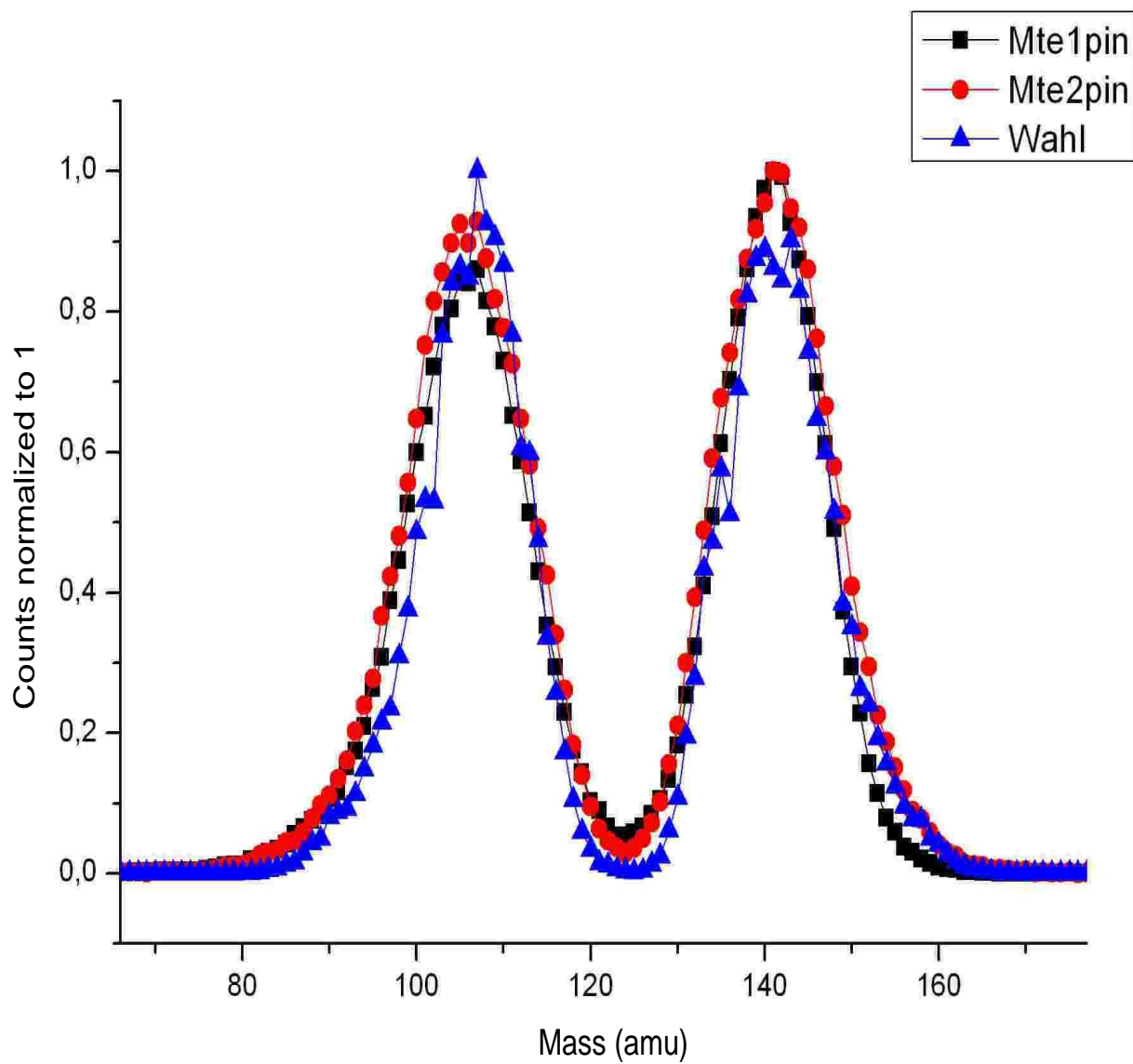


FIG. 4.1. The mass spectra obtained from LIS setup through the true calibration procedure compare to the known mass spectrum from literature [Wah88].

$\langle M_H \rangle$  for PIN1 and PIN2 of LIS setup is compared with the parameters from literature. The standard deviation for both the light and heavy fragments ( $\sigma_L$  and  $\sigma_H$ ) are also shown in Table 4.1. The calculated velocity spectra obtained from PIN1 (Vel1pin) and

TABLE. 4.1. **Parameters obtained from the first experiment using LIS setup.**

Parameter	Average on PIN1	Average on PIN2	Data from [Wah88]
$M_L$ in <i>amu</i>	105.82±0.05	105.76±0.07	106.91
$M_H$ in <i>amu</i>	140.91±0.04	141.28±0.06	141.46
$\sigma_{M_L}$ in <i>amu</i>	6.0	6.0	5.8
$\sigma_{M_H}$ in <i>amu</i>	5.7	5.7	6.2

PIN2 (Vel2pin) are compared with the known spectra from literature [Sch83] and shown in Fig 4.2.

A Comparison of the velocity and energy parameters from our first experiment with results from literature is shown in Table 4.2. In the table, average velocities of the light and heavy fragments are denoted by  $\langle V_L \rangle$  and  $\langle V_H \rangle$  respectively and given in units of *cm/ns*. The average energies of the light and heavy fragments are also given in the table and denoted by  $\langle E_L \rangle$  and  $\langle E_H \rangle$  respectively. The energy parameters obtained from this experiments are compared with the parameters from [Yam07]. The results in Fig 4.2 and Table 4.2 agrees very well with the literature results. The velocity obtained from the time-

TABLE. 4.2. **Comparison of the velocity and energy parameters of the LIS setup with results from literature.**

Parameter	Average on PIN1	Average on PIN2	[Sch83]	[Yam07]
$V_L$ in <i>cm/ns</i>	1.373±0.077	1.373±0.083	1.375±0.007	
$V_H$ in <i>cm/ns</i>	1.031±0.083	1.031±0.088	1.036±0.005	
$\sigma_{V_L}$ in <i>cm/ns</i>	0.064	0.065	0.067	
$\sigma_{V_H}$ in <i>cm/ns</i>	0.072	0.072	0.080	
$E_L$ in <i>MeV</i>	104.46±0.06	104.41±0.06		103.9
$E_H$ in <i>MeV</i>	79.86±0.02	79.61±0.02		80.3
$\sigma_{E_L}$ in <i>MeV</i>	4.47	4.49		5.8
$\sigma_{E_H}$ in <i>MeV</i>	9.66	9.66		6.2

of-flight (TOF) between two MCPs versus the velocity obtained from the TOF between the “start” MCP and PIN1 diode of the first arm is shown in Fig 4.3. The events of interest are marked by a green box which represents our first gate (W1) on the experimental data.

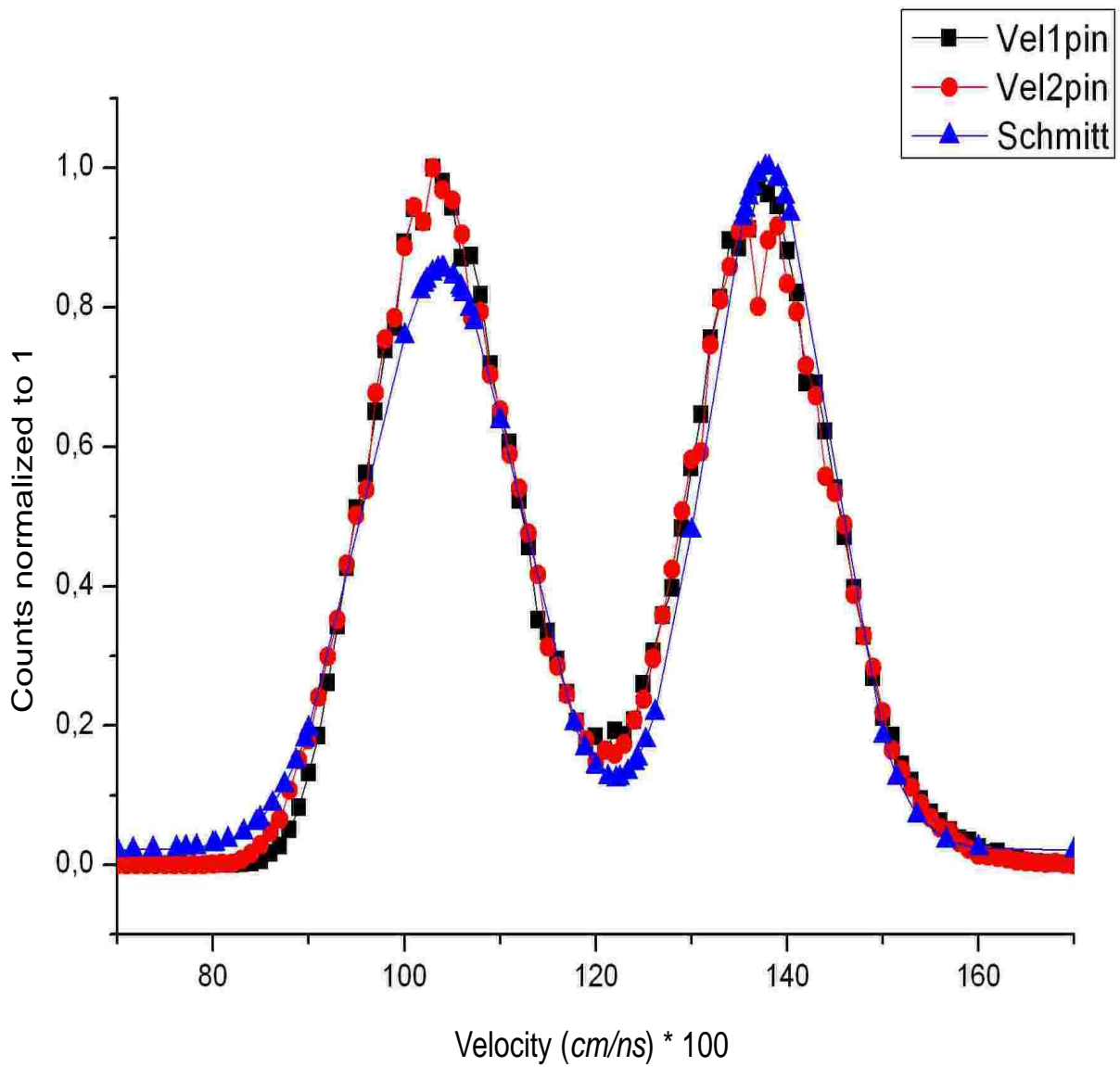


FIG. 4.2. Velocity spectra from the two arms compared with literature spectrum [Sch83].



The events to the left of W1 are due to the scattered fission fragments on the mirror of the “stop” MCP based detector. A similar distribution obtained from the second arm is shown in Fig 4.4 with a similar gate set for the events of interest.

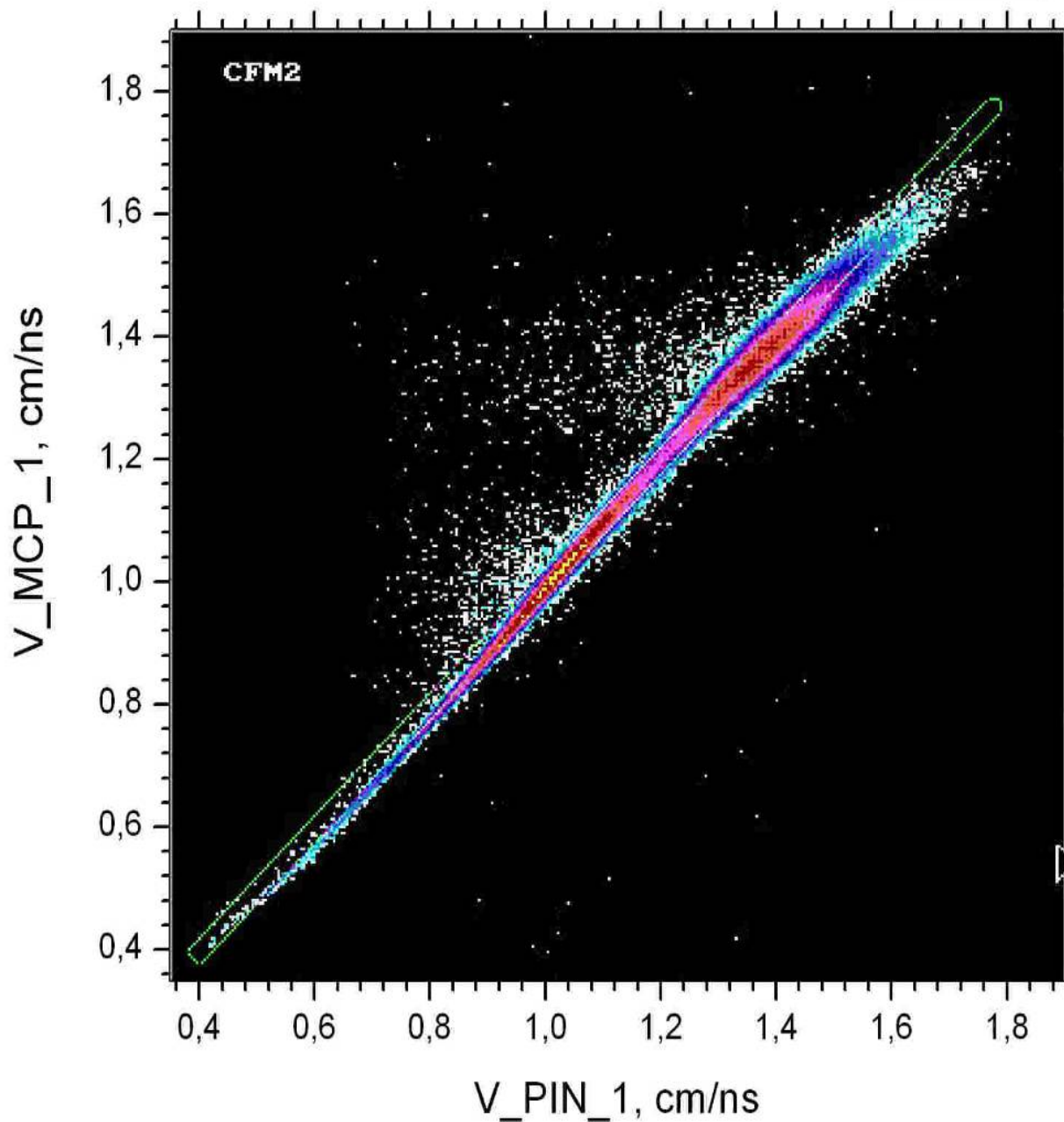


FIG. 4.3. The velocity from the MCP-MCP time of flight versus the velocity from the PIN-MCP time of flight of the first arm.

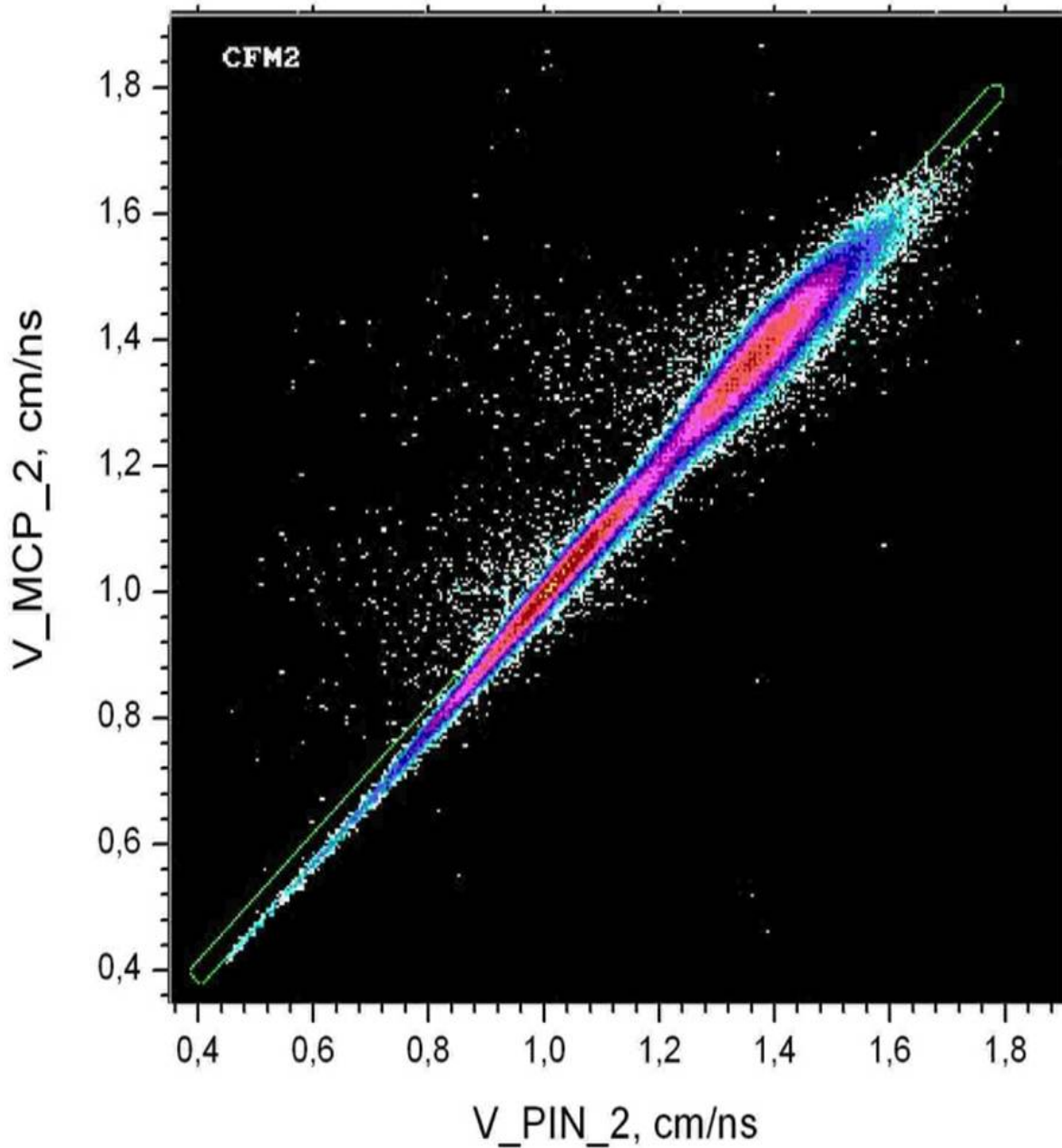


FIG. 4.4. The velocity from the MCP-MCP time of flight versus the velocity from the PIN-MCP time of flight of arm two.

The distribution that shows the mass calculated from the events detected in PIN1 ( $M_{te1}$ ) versus the mass calculated from the events detected in PIN2 ( $M_{te2}$ ) is shown in Fig 4.5. This distribution was obtained using the “first approximation” calibration method as de-

scribed in chapter 3.

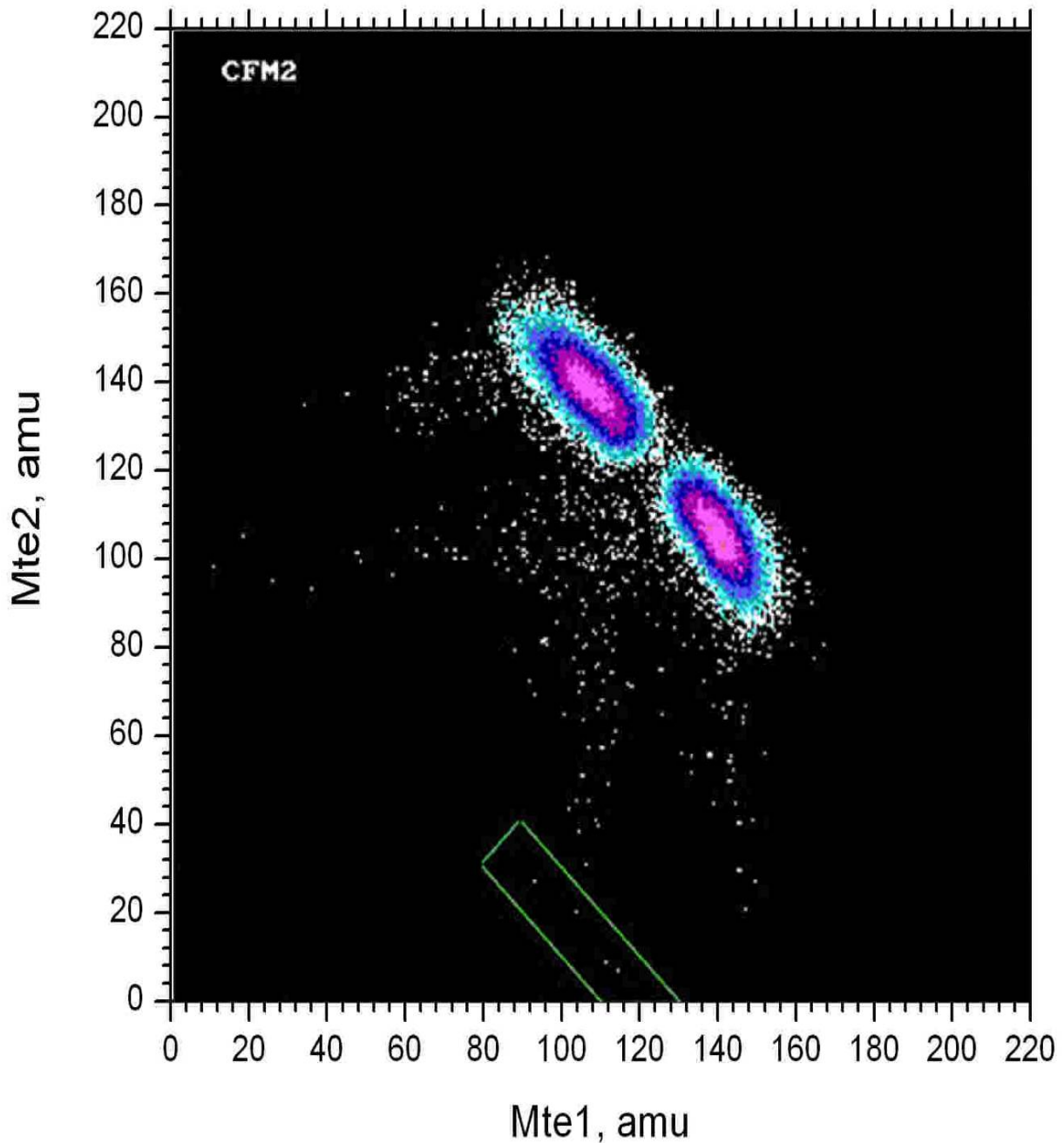


FIG. 4.5. A mass versus mass distribution of the events selected by the W1 and W2 gates.

A specific CCT mode based on the double magic  $Sn$  cluster has been outlined in previous chapters as the key point of investigation. This mode, the “ $Sn$ -lost” CCT mode, is marked

by the green box in Fig 4.5 above. Our results as given above show events linked with this “*Sn*-lost” CCT mode. These results point to the reliability of the LIS setup in studying the “*Sn*-lost” CCT mode. A significant point considering that this mode could possible lead to the new lead radioactivity as discussed in chapter 1.

## 4.3 Conclusion

### 4.3.1 Summary

Two multi-detector registration systems for the study of multi-body decays of heavy nuclei, namely, COMETA (Correlation Mosaics Energy - Time Array) setup and Light Ions Spectrometer (LIS), have been successfully designed and tested. The COMETA setup was designed with the aim of revealing all the CCT partners directly. In order to achieve this, a belt of neutron counters was installed around the “start” detector of the COMETA setup as shown in Fig 2.1.

The optimum configuration to arrange the neutron counters in a belt was determined with the use of the Monte Carlo N-Particle (MCNP) simulation code. The code was also used to determine the detection efficiency of the “neutron belt”. An optimum detection efficiency value of 4.25% was obtained. The procedures involved in the calculation of the detection efficiency have been presented in the following references [Kam10b] [Kam11] [Pya11a] [Pya12].

It was mentioned in chapter 2 that the use of the COMETA spectrometer in the investigation of the CCT mode had two draw backs namely PHD and “plasma delay”. The PHD effect was solved by a specially designed calibration procedure but the “plasma delay” could only be solved by the design of a new spectrometer setup. Success of this calibration procedure to solve the PHD effect can be seen in the data agreement between our experimental mass distribution and the data from literature [Wah88]. Results of our work using this particular calibration procedure are presented in [Mal11].

It was already mentioned that the “plasma delay” effect was solved through the design

of the new spectrometer setup called LIS. This setup was able to reveal the so called “*Sn* lost” CCT mode which is a specific CCT mode based on the lost double magic  $^{132}\text{Sn}$  nucleus. Results from this setup are still to be published.

### 4.3.2 Conclusion

For a number of years the Flerov Laboratory of Nuclear Reactions (FLNR) of the Joint Institute for Nuclear Research (JINR) has conducted studies of the multi-body decays of low excited nuclear systems commonly referred to as Collinear Cluster Tri-partition (CCT). This mode is named as such because it involves three decay partners that fly apart collinearly unlike in conventional binary fission which only involves two decay partners. CCT is energetically more favourable than the conventional binary fission and the full understanding of its mechanism holds new possibilities for future application. While two decay partners were identified directly in previous experiments with the third partner identified through the missing mass method, the aim was always to identify all three partners directly.

The aim of this study was to design, develop and test the new systems of spectrometers aimed at the direct detection of all three decay partners of this rare CCT decay mode. At this point it is known that there are three different types of ternary decays of low excited nuclei, namely, conventional ternary fission, polar emission and collinear cluster tri-partition (CCT). Looking at the polar emission and the CCT, there might be a link between them when the CCT is accompanied by a light charged particle. Based on the two multi-detector registration systems presented in this thesis, a new framework can be followed to compare all the three ternary decays to achieve a unified experimental approach for ternary decay.

### 4.3.3 Future work

Progress achieved in this study on CCT measurements has encouraged us to plan new experiments. One of the planned experiments is making use of the electrostatic guide based VEGA (V-E Guide based Arrangements) Setup at the IBR-2 reactor (installed at the Lab-

---

oratory of Nuclear Problems of the JINR in Dubna, Russia) for the study of collinear products of the multi-cluster decay. The aim of this particular experiment is the detection of the middle-light (masses  $\sim 40amu$ ) CCT products from the  $^{235}U(n_{th}, f)$  and  $^{229}Th(n_{th}, f)$  reactions at the VEGA setup. The other planned experiment is to use LIS and COMETA spectrometers to search for new kinds of cluster decay namely *ternary lead radioactivity*.

# Bibliography

- [Alb69] Alberigi Quaranta A., Taroni A. and Zanarini G., 1969, *Nucl. Instr. And Meth*, **72**, p 72
- [Ale00] Alexandrov A. A. et al., 2000, *Heavy Ion Physics FLNR-JINR Scientific Report 1999-2000*, Russia, Dubna, p 159
- [And65] Andritsopoulos G et al., 1965, *Physics and Chemistry of Fission*, **v1**, IAEA, Vienna, p 481
- [Ber84] Berger J. F. et al., 1984, *Nucl. Phys. A*, **v428**, p 23
- [Boh39] Bohr N. and Wheeler J., 1939, *Phys. Rev.* **56**, p 426
- [Boh55] Bohr N., 1955, *Proc. of the Int. Conf. on the Peaceful Uses of Atomic Energy*, Geneva, **2**, p 151
- [Die73] Diehl H. and Greiner W., 1973, *Phys. Letters B*, **45**, p 35
- [Die74] Diehl H. and Greiner W., 1974, *Nucl. Phys. A*, **229**, p 29
- [Fer34] Fermi E., d'Agostino O., Rasetti F. and Segre E., 1934 *Proc. Roy. Soc. A*, **146**, p 483
- [Fle40] Flerov G. N. and Petrzhak A., 1940, *Zh. Eksp. Teor. Fiz.(russian)*, **10**, p 1013
- [Fle66] Flerov G. N. et al., 1966, *JINR Preprint*, **E7**, p 2924
- [Gon00] Gonnwein F. et al., 2000, *Proc. Seminar on Fission Point dOye IV, Belgium*, *World Scientific*, p 59

- [Gon04] Gonnenwein F., 2004, *Nucl. Phys.*, **A734**, p 213
- [Gon05] Gonnenwein F. et al., 2005, *Europhysics News*, **v36**, p 11
- [Gre47] Green L.L. and Livesey D. L., 1947, *Nature*, **195**, p 332
- [Han78] Hannappel L., Henschel H. and Schmidt R., 1978, *Nucl. Instr. and Meth.*, **151**, p 537
- [Hah39] Hahn O. and Strassmann F., 1939, *Die Naturwissenschaften* **27**, p 11
- [Hil53] Hill D. L. and Wheeler J. A., 1953 *Phys. Rev.* **89**, p 1102
- [Hil89] Hilscher D et al., 1989, *Phys. Rev. Lett.*, **62**, p 1099
- [Iye66] Iyer R. H. and Cobble J. W., 1966, *Phy. Rev. Letters* **17** p 541
- [Jam94] James F., 1994, *Minuit Fucntion Minimization and Error Analysis, Reference Manual*, CERN Geneve, Switzerland
- [Kam03a] Kamanin D. V., Pyatkov Yu. V., Alexandrov A. A., Alexandrova I. A., Vasko V. M., Zhuchko V. E., Mitrofanov S. V. and Tishchenko V. G., 2003, *FLNR JINR Scientific Report, Heavy Ion Physics* p 221
- [Kam03b] Kamanin D. V. et al., 2003, *Physics of Atomic Nuclei*, **66** p 1655
- [Kam04] Kamanin D. V. et al., 2004, *Proc. Int. Symp. on Exotic Nuclei*, Peterhof, Russia, p 588
- [Kam08] Kamanin D. V., Pyatkov Yu. V, Tyukavkin and Kopatch Yu. N., 2008, *Int. Journal of Modern Physics* **17**, p 2250
- [Kam10a] Kamanin D. V. et al., 2010, *Physics of Particles and Nuclei Letters* **7**, p 121
- [Kam10b] Kamanin D. V. et al., 2010, *Proc. Int. Symposium of Exotic Nuclei*, Russia, Sochi, p 385
- [Kam11] Kamanin D. V. et al., 2011 *Presented in the 19th Int. Seminar on Interaction of Neutrons with Nuclei*, Russia, Dubna



- [Kam11a] Kamanin D. V. et al., 2011 *Presented by Malaza V.D. in the 19th Int. Seminar on Interaction of Neutrons with Nuclei*, Russia, Dubna
- [Kat58] Katz L., Baerg A. P. and Brown F., 1958, *Proc. of the Second UN Int. Conf. on the Peaceful Uses of Atomic Energy*, Geneva, **15**, p 188
- [Kim93] Kim Y. S. et al., 1993, *Nucl. Instr. and Meth.*, **A329**, p 403
- [Leo94] Leo W. R., 1994, *Techniques for Nuclear and Particle Physics Experiments, A How-to Approach*, **Springer**, p 81
- [Mal11] Malaza V.D. et al., 2011, *Proc. of 56th Annual Conf of the South African Institute of Physics*, Pretoria p 385
- [Mar67] Mariscotti M. A., 1967, *Nucl. Instr. and Meth.*, **v50** p 309
- [Mei39] Meitner L. and Frisch O. R., 1939, *Die Naturwissenschaften*, **143**, p 239
- [Mos71] Moszynski M. and Bengtson B., 1971, *Nucl. Instr. and Meth*, **91**, p 73
- [Mug63] Muga M. L., 1963, *Phy. Rev. Letters*, **11**, p 129
- [Mug67] Muga M. L. et al., 1963, *Phy. Rev. Letters*, **18**, p 404
- [Mul97] Mulgin S. et al., 1997, *NIM A 388*, p 254.
- [Nei80] Neidel H. O. and Henschel H., 1980, *Nucl. Instr. and Meth.* **178**, p 137
- [Nei83] Neidel H. O. and Henschel H., 1983, *Nucl. Instr. and Meth.* **212**, p 299
- [Now82] Nowicki L. et al., 1982, *Nuclear Physics*, **A375**, p 186
- [Obu68] Obukhov A. I. and Perfilov N. A., 1968, *Soviet Physics Uspekhi*, **10**, p 559
- [Oed83] Oed A. et al., 1983, *Nucl. Instr. and Meth.*, **205**, p 451
- [Ort98] Ortlepp H. G. et al., 1998, *Nucl. Instr. and Meth.* **A403**, p 65
- [Pas09] Pashkevich V. et al., 2009, *Int. Journal of Modern Physics* **18**, p 907
- [Per57] Perfilov N. A., 1957, *Physics of Nuclear Fission*, Atomizdat, Russia, p 98

- [Pia70] Piasecki E., Dakowski M., Krogulski T., Tys J. and Chwaszczewaka J., 1970, *Physics Letters*, **B33** p 568
- [Pia73] Piasecki E. and Blocki J., 1973, *Nucl. Phys*, **A208**, p 628
- [Pia74] Piasecki E. and Blocki J., 1974, *Acta Phys. Pol.* **B5**, p 247
- [Pia75] Piasecki E., Sowinski M., Nowicki L., Kordyasz A., Cieslak E. and Czarnacki W., 1975, *Nuclear Physics*, **A255**, p 387
- [Pia80] Piasecki E. and Nowicki L., 1980, *Proc. Symp. on Physics and Chemistry of Fission*, Julich, **v2**, p 193
- [Poe02] Poenary D. N. et al., 2002, *Proc. Symp. On Nuclear Cluster*, German, p 283
- [Pre41] Present R. D., 1941, *Phy. Rev*, **59**, p 466
- [Pya97] Pyatkov Yu. V. et al., 1997, *Nucl. Phys. A*, **v624**, p 140
- [Pya00] Pyatkov Yu. V. et al., 2000, *Proc. Int. Conf. on Nuclear Spectroscopy "Nuclear Shells 50 years"*, Russia, Dubna, p 144
- [Pya02] Pyatkov Yu. V. et al., 2002, *Nucl. Instr. and Meth. A*, **v488**, p 381
- [Pya03] Pyatkov Yu. V. et al., 2003, *Proc. XVIth Int. Workshop on Physics of Nuclear Fission*, Russia, Obninsk
- [Pya04] Pyatkov Yu. V. et al., 2004, *Physics of Atomic Nuclei*, **v67**, p 1726
- [Pya07a] Pyatkov Yu. V. et al., 2007, *Romanian Reports in Physics*, **59**, p 388
- [Pya07b] Pyatkov Yu. V. et al., 2007, *Proc. 14th Int. Seminar on Interaction of Neutrons with Nuclei*, Russia, Dubna, p 134
- [Pyat07c] Pyatkov Yu. V. et al., 2007 *Proc. Int. Symp. On Exotic Nuclei*, **912**, p 144
- [Pya08] Pyatkov Yu. V. et al., 2008, *Proc. 6th Int. Conf. on Dynamical Aspects of Nuclear Fission*, Slovak Republic, Smolenice Castle, p 248
- [Pya10] Pyatkov Yu. V. et al., 2010, *European Physics Journal* **A45** p 29

- [Pya10a] Pyatkov Yu. V. et al., 2010, *Proc. Int. Symp. On Exotic Nuclei*, Sochi, Russia, p 393
- [Pya11] Pyatkov Yu. V. et al., 2011, *Bulletin of the Russian Academy of Science*, **v75**, p 949
- [Pya11a] Pyatkov Yu. V. et al., 2011, *Int Journal of Mordern Phys. E*, **v20** N04, p 1008
- [Pya12] Pyatkov Yu. V. et al., 2012, *Eur. Phy. J.*, **A**, p 48
- [Ron02] Ronen Y., 2002, *Annals of Nuclear Energy*, **29**, p 1013
- [Roc04] Rocman D. et al., 2004, *Nucl. Phys. A*, **v735**, p 3
- [Sch83] Schmidt R. and Henkel H., 1983, *Nucl. Phys. A* **395**, p 15
- [Sem01] Semenov Yu. B. et al., 2001, *Heavy Ion Physics, FLNR JINR Scientific Report 1999 - 2000*, p 196
- [Shu06] Shultis J.K. and Faw R.E., 2006, *An MCNP Primer*.
- [Sok97] Sokol E. A. et al., 1997, *Nucl. Instr. and Meth.* **A400** p 96
- [Sto66] Stoenner R. W. and Hillman M., 1966, *Phys. Rev.* **142**, p 943
- [Str63] Strutinsky V. M. et al., 1963, *Nucl. Phys.*, **46**, p 639
- [Swi58] Swiatecki W. J., 1958, *Proc. of the Second UN Int. Conf. on the Peaceful Uses of Atomic Energy*, Geneva, p 651
- [Tsi47] Tsien San-Tsiang et al., 1947, *Phy. Rev.*, **71**, p 382
- [Tyu03] Tyukavkin A. N. et al., 2003, *Presented at the XVIth Int. Workshop on Phys. of Nuclear Fission*, Obninsk, Russia
- [Van58] Vandenbosch R., Thomas T. D., Vandenbosch S. E., Glass R. A. and Seaborg G. T., 1958, *Phys. Rev.* **111**, p 1358
- [Wah88] Wahl C., 1988, *Atomic data and nuclear data tables*, **39**, p60
- [Wil76] Wilkins B.D. et al., 1976, *Phys. Rev. C*, **v14**, p 1832

- 
- [Yam07] Yamaletdinov S, 2007, *Studies of Exotic Decay Modes in Fission of Heavy Elements*, PhD Thesis, Department of Physics, University of Jyväskylä, Finland
- [Zhu07] Zhuchko V. E., Kamanin D. V. and Kuznetsova E. A., 2007, *Proc. 14th Int. Seminar on Interaction of Neutrons with Nuclei*, Russia, Dubna, p 236